

## $d'$ dibaryon in a colored cluster model

A. J. Buchmann,<sup>1,\*</sup> Georg Wagner,<sup>2,†</sup> and Amand Faessler<sup>1,‡</sup>

<sup>1</sup>*Institut für Theoretische Physik, Universität Tübingen, Auf der Morgenstelle 14, D-72076 Tübingen, Germany*

<sup>2</sup>*Centre for the Subatomic Structure of Matter (CSSM), University of Adelaide, S.A. 5005 Adelaide, Australia*

(Received 21 January 1997)

The mass and wave function of a six-quark system with quantum numbers  $J^P=0^-, T=0$ , called  $d'$ , are calculated. We use a colored diquark-tetraquark cluster model for the six-quark wave function. A constituent quark model Hamiltonian with a two-body confinement potential, and residual one-gluon, one-pion, and one- $\sigma$  exchange interactions is used. The complications due to the quark exchange interactions between tetraquark and diquark clusters (Pauli principle) are taken into account within the framework of the resonating group method. The calculated  $d'$  mass is some 350 MeV above the empirical value if the same two-body confinement strength as in the nucleon and  $\Delta$  is used. This paper also examines the validity of the usual assumption of a universal two-quark confinement strength. We propose that the effective two-body confinement strength in an exotic six-quark system, such as the  $d'$ , could be weaker than in a single baryon. The weaker confinement hypothesis leads to a  $d'$  mass of  $M_{d'}=2092$  MeV and a  $d'$  radius of  $r_{d'}=1.53$  fm. [S0556-2813(98)06905-2]

PACS number(s): 14.20.Pt, 12.39.Pn, 12.39.Jh, 12.40.Yx

### I. INTRODUCTION

First indications for the existence of the  $d'$  dibaryon came from the narrow peak observed in the pionic ( $\pi^+, \pi^-$ ) double charge exchange (DCX) reaction on nuclei. At an incident pion energy of  $T_\pi \sim 50$  MeV and forward pion scattering angles  $\Theta = 5^\circ$ , the DCX cross section, for example for  $\pi^+ + {}^{12}\text{C} \rightarrow {}^{12}\text{O} + \pi^-$ , displays a narrow peak [1–3]. Because of charge conservation, the DCX reaction involves at least two nucleons within the nucleus, and it has been shown that the DCX reaction is therefore very sensitive to short-range  $NN$  correlations [4]. The possible importance of explicit quark degrees of freedom in DCX at 50 MeV and forward angles was pointed out some time ago [5]. In the meantime, dedicated DCX experiments [3,6,7] on a large number of light and medium heavy nuclei ranging from  ${}^7\text{Li}$  to  ${}^{56}\text{Fe}$  have unambiguously confirmed the existence of a narrow resonancelike structure at this pion energy and angle.

While conventional DCX calculations [8,9] have so far been unable to explain these experimental results, the assumption of a single narrow baryon number  $B=2$  resonance with total spin, parity  $J^P=0^-$ , isospin  $T=\text{even}$ , a resonance energy of  $M_{d'}=2065$  MeV, and a free decay width of  $\Gamma_{\pi NN} \approx 0.5$  MeV works extremely well in describing all available DCX data [3,10]. To exclude a possible nuclear structure explanation [11], experimentalists have searched for the  $d'$  in proton-proton collisions, e.g., in  $pp \rightarrow pp\pi^+\pi^-$ . A  $4\sigma$  enhancement over the background exactly at the  $d'$  position has been observed in the  $\pi^-pp$  invariant mass spectrum [12].

Two alternative models for the structure of the  $d'$  have been discussed in the literature. If the  $d'$  is predominantly composed of two *colorless* three-quark clusters, it could be a

resonance in the  $NN^*$  channel, where  $N^*$  is the first negative parity excitation of the nucleon at 1535 MeV. Because the empirical mass of the  $d'$  is far below the  $N^*N$  threshold, this requires an enormous binding energy for the bound  $NN^*$  system. This interpretation is reminiscent of the deep-lying bound states in the Moscow  $NN$  potential [13]. The  $d'$  dibaryon has also been interpreted as an isospin  $T=2N\Delta$  resonance [14], a  $\pi NN$  state with  $T=2$  [15], and most recently as a  $\pi NN$  state in the isospin  $T=0$  channel [16], located at 2018 MeV.

It is important to note that due to its quantum numbers ( $L=1, S=1, T=0$ ), the  $d'$  cannot be composed of two ground-state nucleons because such a state is Pauli forbidden. The Pauli principle demands that the quantum numbers of a two-nucleon system satisfy  $(-1)^{L+S+T} = -1$ . Therefore, the  $d'$  cannot simply decay into two nucleons. A decay into two nucleons is possible only if a pion or a photon is emitted simultaneously. The correspondingly small phase space naturally explains the small width of the  $d'$ .

On the other hand, quantum chromodynamics (QCD) does not preclude the possibility that the quarks in the initial  $\pi NN$  system rearrange themselves into energetically favorable but unobservable *colored* clusters [17]. This idea is not new. Several scenarios for the arrangement of quarks and antiquarks into colored clusters combining to an overall color neutral  $B=2$  system have been proposed [18–21]. An early suggestion is the “demon” deuteron, which is a  $J^P=0^-, T=0$  dibaryon consisting of three pairs of diquarks [22]. Other partitionings have been studied in the stringlike bag model [23,24]. This model predicts that a rotating ( $L=1$ ) dumbbell-like configuration with a colored diquark ( $q^2$ ) and tetraquark ( $q^4$ ) cluster connected by a flux tube of color-electric-field lines is the state with lowest energy for a six-quark system with  $d'$  quantum numbers. Figure 1 shows how such a  $q^2-q^4$  cluster system could be formed from the initial  $\pi NN$  state.

A shortcoming of the stringlike bag model [23,24] is that it employs rigid impenetrable tetraquark and diquark clusters

\*Electronic address: alfons.buchmann@uni-tuebingen.de

†Electronic address: gwagner@physics.adelaide.edu.au

‡Electronic address: amand.faessler@uni-tuebingen.de

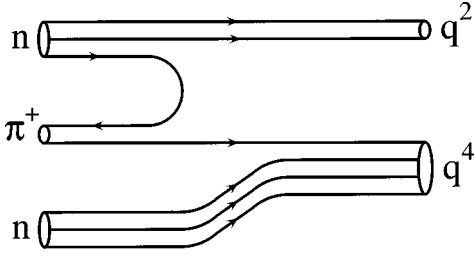


FIG. 1. The formation of a compound six-quark system from the initial  $\pi^+ nn$  system. The  $\bar{d}$  quark in the  $\pi^+$  annihilates with a  $d$  quark in one of the neutrons leading to a  $q^2-q^4$  clusterized six-quark state. In the stringlike bag model, colored diquark and tetraquark clusters are bound together by a color-electric flux-tube (string), which is rotating with angular momentum  $L=1$ . In the present model, the relative  $q^2-q^4$  wave function is calculated from the Hamiltonian of Eq. (1).

at the ends of a rotating color string. This model neither allows that the clusters merge into a single compound six-quark bag nor that they exchange quarks. Only the quarks within the individual clusters are antisymmetrized but not the quarks belonging to different clusters. Therefore, the stringlike bag model does not fully respect the Pauli principle. The stringlike bag model is a good approximation only for high angular momentum states ( $L>5$ ) [25]. In this case, the system is fairly elongated because of centrifugal forces, and the probability of cluster overlap is small. However, for a low-lying  $L=1$  excitation, such as the  $d'$ , one expects considerable overlap between the clusters and a substantial amount of quark exchange between them. We are sceptical that an  $L=1$  state is sufficiently stretched for the stringlike bag model treatment to be valid. The condition of validity is  $l>2R_0$  [23], where  $l$  is the length and  $R_0$  is the radius of the color flux tube connecting the colored quark clusters. For the  $d'$ , this condition is barely satisfied, and one anticipates corrections to the bag model prediction  $M_{d'} \approx 2100$  MeV [23,24].

The purpose of this work is to study the dynamics of diquark-tetraquark relative motion using a microscopic quark model Hamiltonian and the resonating group method (RGM). The model used here accurately reproduces the mass of the deuteron, which is the only established dibaryon. By comparing the RGM solutions with our previous results [26–28], employing a single  $s^5p^1$  six-quark ‘‘bag,’’ we can test the validity of the assumption underlying the stringlike bag model, namely that the  $d'$  is a stretched  $q^2-q^4$  system. In the present work, all complications arising from the quark exchange interactions (Pauli principle) are rigorously taken into account, and their effect on the  $d'$  mass and wave function is investigated in some detail. In addition, the present paper critically examines the validity of the assumption of a universal two-body confinement strength and explores how a possible reduction of the effective confinement strength in a compound six-quark system affects the mass and the size of the  $d'$ .

The paper is organized as follows. Section II provides a short description of the chiral quark model used. Section III presents the six-quark resonating group method approach. Section IV discusses the numerical results for the mass and size of the  $d'$  for several confinement models and compares the present predictions to those of the single-bag shell model

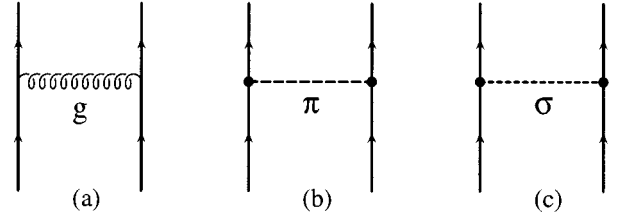


FIG. 2. The residual (a) one-gluon, (b) one-pion, and (c) one- $\sigma$  exchange interactions. The finite size of the quark-meson vertex described by the cutoff  $\Lambda$  is indicated by a small black dot.

and the stringlike bag model. Our summary and conclusions are given in Sec. V. The Appendix contains explicit expressions of the norm and Hamiltonian kernels needed for the solution of the RGM equation of motion.

## II. THE CHIRAL CONSTITUENT QUARK MODEL

In the chiral constituent quark model a system of  $n$  quarks with equal masses  $m_q=313$  MeV  $=m_N/3$  [SU $_F(2)$ ] is described by the Hamiltonian

$$H = \sum_{i=1}^n \left( m_q + \frac{\mathbf{p}_i^2}{2m_q} \right) - \frac{\mathbf{P}^2}{n(2m_q)} + \sum_{i<j}^n V^{\text{conf}}(\mathbf{r}_i, \mathbf{r}_j) + \sum_{i<j}^n V^{\text{res}}(\mathbf{r}_i, \mathbf{r}_j), \quad (1)$$

where  $\mathbf{r}_i, \mathbf{p}_i$  are the spatial and momentum coordinates of the  $i$ th quark and  $\mathbf{P}$  is the total momentum of the  $n$ -quark system. The exact removal of the center-of-mass kinetic energy by the third term represents an important advantage of the present approach.

The residual interactions  $V^{\text{res}} = V^{\text{OGEP}} + V^{\text{OPEP}} + V^{\text{OSEP}}$  between quarks shown in Fig. 2 model the most relevant properties of QCD, such as asymptotic freedom at high, and spontaneous chiral symmetry breaking at low energies. The one-gluon exchange potential [29]

$$V^{\text{OGEP}}(\mathbf{r}_i, \mathbf{r}_j) = \frac{\alpha_s}{4} \boldsymbol{\lambda}_i \cdot \boldsymbol{\lambda}_j \left\{ \frac{1}{r} - \frac{\pi}{m_q^2} \left( 1 + \frac{2}{3} \boldsymbol{\sigma}_i \cdot \boldsymbol{\sigma}_j \right) \delta(\mathbf{r}) \right\} \quad (2)$$

provides an effective quark-quark interaction that has the spin-color structure of QCD at short distances. Here,  $\mathbf{r} = \mathbf{r}_i - \mathbf{r}_j$ , and  $\boldsymbol{\sigma}_i$  is the usual Pauli spin matrix. The  $\boldsymbol{\lambda}_i$  represent the Gell-Mann matrices of SU(3) $_{\text{color}}$ . We neglect tensor and spin-orbit forces, which have been shown to be of minor importance for the  $d'$  [27]. Only central potentials are considered in this work.

The spontaneous breaking of chiral symmetry of low-energy QCD by the physical vacuum is responsible for the constituent quark mass generation [30], as well as for the appearance of pseudoscalar and scalar collective excitations of the vacuum ( $\pi$  and  $\sigma$  fields). These collective degrees of freedom couple directly to the constituent quarks. In the present quark model with two quark flavors, this mechanism is modeled by regularized one-pion and one- $\sigma$  exchange potentials between constituent quarks [31–33]:

$$V^{\text{OPEP}}(\mathbf{r}_i, \mathbf{r}_j) = \frac{g_{\pi q}^2}{4\pi} \frac{1}{12m_q^2} \frac{\Lambda_\pi^2}{\Lambda_\pi^2 - m_\pi^2} \boldsymbol{\tau}_i \cdot \boldsymbol{\tau}_j \boldsymbol{\sigma}_i \cdot \boldsymbol{\sigma}_j \nabla_r^2 \times \left( \frac{e^{-m_\pi r}}{r} - \frac{e^{-\Lambda_\pi r}}{r} \right), \quad (3)$$

$$V^{\text{OSEP}}(\mathbf{r}_i, \mathbf{r}_j) = -\frac{g_{\sigma q}^2}{4\pi} \frac{\Lambda_\sigma^2}{\Lambda_\sigma^2 - m_\sigma^2} \left( \frac{e^{-m_\sigma r}}{r} - \frac{e^{-\Lambda_\sigma r}}{r} \right), \quad (4)$$

with

$$\frac{g_{\sigma q}^2}{4\pi} = \frac{g_{\pi q}^2}{4\pi}, \quad m_\sigma^2 \approx (2m_q)^2 + m_\pi^2, \quad \Lambda_\pi = \Lambda_\sigma \equiv \Lambda. \quad (5)$$

The  $\pi q$  coupling constant  $g_{\pi q}^2/4\pi$  is related to the  $\pi N$  coupling constant  $g_{\pi N}^2/4\pi$  by  $g_{\pi q} = (3/5)(m_q/m_N)g_{\pi N}$  with  $g_{\pi N} = 13.19$  [34]. The  $\pi q$  cutoff mass  $\Lambda$  describes the finite size of the constituent quark due to its pion cloud

$$r_q^2 = \frac{3}{\Lambda^2}. \quad (6)$$

Here, we choose  $\Lambda = 4.2 \text{ fm}^{-1}$  which gives  $r_q = 0.41 \text{ fm}$ , and leads to a soft  $\pi N$  form factor [35]. The  $\sigma$  parameters are fixed by Eq. (5). In particular we use  $m_\sigma = 626 \text{ MeV}$ .

The usefulness and phenomenological success of the model has previously been demonstrated. For example, the chiral constituent quark model has recently been used to calculate the positive parity spectrum of the nucleon and various electromagnetic observables of the ground-state octet and decuplet baryons and their excited states [35]. It has also been applied to calculate the properties of the deuteron [33],  $NN$  phase shifts [32,33], hyperon-hyperon interactions, as well as the  $H$  particle [36].

### A. Confinement models

There are mainly two types of confinement potentials discussed in the literature, namely the two-body confinement potential introduced by Lipkin [37], and the color flux tube (string) model of confinement. In the color flux tube model, the color string describes the hidden gluon degrees of freedom that are necessary to preserve color gauge invariance of the underlying field theory. In a many-quark system, or in the interaction region of hadron-hadron collisions, the strings can change their positions and oscillate between different configurations. This continuous flipping of color strings can be effectively described in the flip-flop model [38], which has been introduced to avoid the long-range color van der Waals forces in hadron-hadron interactions. In the flip-flop model, the confinement interaction between any pair of quarks depends on the position of the remaining quarks; it thus contains many-body operators.

Here, for reasons of simplicity, we consider several *two-body* confinement potential models of Lipkin-type, which differ in their radial dependence (see Fig. 3) but not in their color structure. We should keep in mind that these potentials may not be adequate for describing the complicated dynamics of changing color strings in a many-quark system.

In the constituent quark model one often takes a simple quadratic confinement potential:

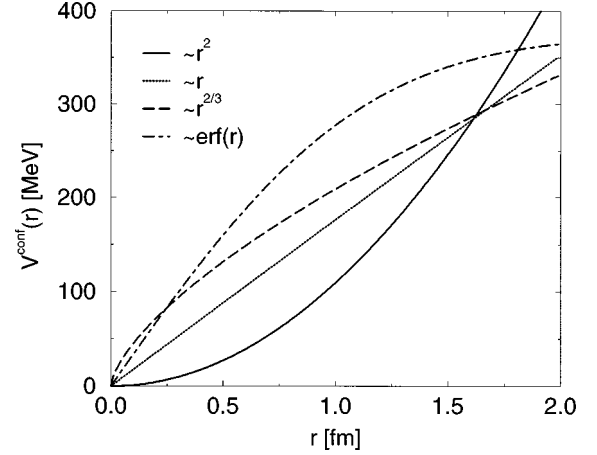


FIG. 3. The radial dependence of typical confinement models in the nucleon.

$$V_q^{\text{conf}}(\mathbf{r}_i, \mathbf{r}_j) = -a_c^{(q)} \boldsymbol{\lambda}_i \cdot \boldsymbol{\lambda}_j (\mathbf{r}_i - \mathbf{r}_j)^2. \quad (7)$$

Later we use this model to argue that the usual assumption of a universal two-body confinement strength  $a_c^{(q)}$  is too restrictive and may not be adequate for compact six-quark systems.

Lattice-QCD calculations find that the quark-antiquark potential of QCD is linear:

$$V_l^{\text{conf}}(\mathbf{r}_i, \mathbf{r}_j) = -a_c^{(l)} \boldsymbol{\lambda}_i \cdot \boldsymbol{\lambda}_j |(\mathbf{r}_i - \mathbf{r}_j)|. \quad (8)$$

The linear form has also been used in our previous calculation [26,27] using the translationally invariant shell model (TISM).

Another interesting parametrization is the  $r^{2/3}$  confinement potential:

$$V_r^{\text{conf}}(\mathbf{r}_i, \mathbf{r}_j) = -a_c^{(r)} \boldsymbol{\lambda}_i \cdot \boldsymbol{\lambda}_j |(\mathbf{r}_i - \mathbf{r}_j)|^{2/3}. \quad (9)$$

In Ref. [39] it is shown that a  $r^{2/3}$  confinement potential and a color-Coulomb potential leads in the framework of the nonrelativistic Schrödinger equation to the observed linear Regge trajectories of hadron masses.

Finally, we consider the color-screened error-function confinement [40]:

$$V_e^{\text{conf}}(\mathbf{r}_i, \mathbf{r}_j) = -a_c^{(e)} \boldsymbol{\lambda}_i \cdot \boldsymbol{\lambda}_j \text{erf}(\mu r), \quad \text{erf}(x) = \frac{2}{\sqrt{\pi}} \int_0^x e^{-z^2} dz. \quad (10)$$

This potential rises linearly for small  $r$ , but as a result of quark-antiquark pair creation (color screening) grows only weakly for intermediate  $r$  and finally goes to a constant value at large  $r$  (see Fig. 3). Lattice calculations show [40] that such a behavior of the effective quark-quark potential arises if quark-antiquark loops are taken into account. The inverse of  $\mu$  is called color-screening length for which we take  $1/\mu = 0.8 \text{ fm}$ . This potential has recently been used by Zhang *et al.* [41]. Alternatively, an exponential form  $V_{\text{exp}}^{\text{conf}} = [1 - \exp(-\mu r^2)]$  that matches the  $r^2$  behavior for small  $r$  has been suggested and used by Wang *et al.* [42].

### B. Determination of the parameters

For the nucleon and  $\Delta$  wave functions, we use  $s^3$  harmonic-oscillator ground-state wave functions  $\Phi_{N(\Delta)}$

$$|\Phi_{N(\Delta)}\rangle = \left( \frac{1}{\sqrt{3}\pi b_3^2} \right)^{3/2} \exp(-[\boldsymbol{\rho}^2/(4b_3^2) + \boldsymbol{\lambda}^2/(3b_3^2)]) |ST\rangle^{N(\Delta)} \times |[111]_{\text{color}}\rangle^{N(\Delta)}, \quad (11)$$

where the Jacobi coordinates  $\boldsymbol{\rho}$  and  $\boldsymbol{\lambda}$  are defined as  $\boldsymbol{\rho} = \mathbf{r}_1 - \mathbf{r}_2$  and  $\boldsymbol{\lambda} = \mathbf{r}_3 - (\mathbf{r}_1 + \mathbf{r}_2)/2$ . The harmonic-oscillator parameter  $b_3$  describes the mean-square (ms) matter radius of the nucleon. The matter radius is defined with respect to the center-of-mass coordinate  $\mathbf{R}_N$  of the nucleon and is given as

$$r_N^2 = \left\langle \Phi_N \left| \frac{1}{3} \sum_{i=1}^3 (\mathbf{r}_i - \mathbf{R}_N)^2 \right| \Phi_N \right\rangle = b_3^2.$$

As usual, the parameters of the Hamiltonian of Eq. (1) are fitted to the nucleon and  $\Delta$  ground-state masses. The masses of the  $N$  and  $\Delta$  are calculated as expectation values of the Hamiltonian of Eq. (1) between baryon ground-state wave functions  $\Phi_{N(\Delta)}$ . Imposing  $m_q = 313$  MeV and  $\Lambda = 4.2$  fm $^{-1}$ , the parameters  $a_c^{(3)}$ ,  $\alpha_s$ , and  $b_3$  are determined by the requirement that the  $N(939)$  and  $\Delta(1232)$  masses are reproduced, and that the nucleon mass is stable with respect to variations in  $b_3$ :

$$M_N(b_3) = 3m_q = 939 \text{ MeV},$$

$$M_\Delta - M_N = 293 \text{ MeV}, \quad \frac{\partial M_N(b_3)}{\partial b_3} = 0. \quad (12)$$

Although the three coupled equations (12) for the parameters  $a_c^{(3)}$ ,  $\alpha_s$ , and  $b_3$  are nonlinear,  $a_c^{(3)}$  is predominantly determined by the requirement that the nucleon has its physical mass  $M_N = 939$  MeV,  $\alpha_s$  by the mass difference  $M_\Delta - M_N$ , and  $b_3$  by the stability condition  $\partial M_N(b_3)/\partial b_3 = 0$ . The parameters for the different confinement models as determined by Eq. (12) are shown in Table I. Parameter sets I–III are obtained with the quadratic confinement of Eq. (7) and sets IV, V, VI are obtained with the linear,  $r^{2/3}$ , and error-function confinement of Eqs. (8)–(10), respectively.

One can qualitatively understand the trend in the values of the parameters  $a_c^{(3)}$ ,  $\alpha_s$ , and  $b_3$  for the different confinement models by considering the sequence quadratic (set II), linear (set IV),  $r^{2/3}$  (set V), and error-function (set VI) confinement for the case of the nucleon (see Fig. 3). One observes that the stronger the confinement potential grows at small distances, the further out the nucleon wave function (larger  $b_3$ ) extends, in order to minimize the nucleon mass. With increasing  $b_3$ , the importance of the one-pion-exchange interaction decreases, and the contribution of the one-gluon-exchange to the  $N\Delta$  mass splitting—hence  $\alpha_s$ —must increase correspondingly. Finally, because the kinetic energy contribution to the nucleon mass is lower for larger nucleon sizes ( $b_3$ ), a bigger confinement strength  $a_c^{(3)}$  is needed to fit the experimental nucleon mass  $M_N = 939$  MeV.

TABLE I. Quark model parameters. Sets I–III are obtained for the quadratic confinement potential ( $Q$ ) of Eq. (7). Set I: without  $\pi$ - and  $\sigma$ -exchange potentials. Set II: with regularized  $\pi$ - and  $\sigma$ -meson exchange potentials. Set III: same as set II but with reduced confinement strength in the six-quark sector. Set IV: with linear confinement (L) of Eq. (8) instead of quadratic confinement. Set V: with  $r^{2/3}$  confinement interaction (R) of Eq. (9). Set VI: with the color-screened error-function confinement (E) of Eq. (10) using an inverse screening length of  $1/\mu = 0.8$  fm. In columns 5 and 6 we list the confinement strength  $a_c^{(3)}$  as determined from the nucleon mass and the confinement strength  $a_c^{(6)}$  employed for the calculation of the dibaryon mass and wave function as discussed in Sec. IV.

Conf.	Set	$b_3$ (fm)	$\alpha_s$	$a_c^{(3)}$	$a_c^{(6)}$
$Q$	I	0.603	1.540	24.94 MeV/fm $^2$	$= a_c^{(3)}$
$Q$	II	0.595	0.958	13.66 MeV/fm $^2$	$= a_c^{(3)}$
$Q$	III	0.595	0.958	13.66 MeV/fm $^2$	5.00 MeV/fm $^2$
$L$	IV	0.609	1.060	22.03 MeV/fm	$= a_c^{(3)}$
$R$	V	0.617	1.122	26.12 MeV/fm $^{2/3}$	$= a_c^{(3)}$
$E$	VI	0.648	1.374	46.70 MeV	$= a_c^{(3)}$

### III. A COLORED DIQUARK-TETRAQUARK CLUSTER MODEL OF THE $d'$ DIBARYON

In the DCX reaction, the incident pion and the two correlated nucleons may come sufficiently close for the quarks to make use of the additional possibilities provided by their color degree of freedom. In the interaction region, there are several possibilities to make an overall color singlet. The quarks could clusterize into two color singlets, two color triplets, two color sextets, and two color octets:

$$(\mathbf{1} \otimes \mathbf{1})^1; \quad (\bar{\mathbf{3}} \otimes \mathbf{3})^1; \quad (\mathbf{6} \otimes \bar{\mathbf{6}})^1; \quad (\mathbf{8} \otimes \mathbf{8})^1.$$

We recall that a  $q^3 - q^3$  clusterization of the  $d'$  with *colorless* three-quark clusters is either not allowed by quantum numbers (Pauli principle) or by energy considerations. For example, a  $N(939)N(939)$  clusterization with relative angular momentum  $L=1$  is not allowed by the Pauli principle. Similarly, an  $N\Delta$  system with  $L=1$  can only have isospin  $T=2$ , while present experimental results seem to favor the  $T=0$  assignment [43]. Furthermore, the energy of an  $L=0$   $N(939)N^*(1535)$  system, where the negative parity resides inside one cluster, is far above the experimental  $d'$  mass. A recent quark cluster model calculation has found no evidence for a deeply bound state in this system [44]. Therefore, a  $N(939)N^*(1535)$  dibaryon decays strongly into  $NN\pi$ . It has a large width and thus cannot be a viable candidate for the  $d'$ . Thus, the  $d'$  is presumably not a state which is predominantly composed of two colorless three-quark clusters.

In the stringlike bag model, the color-triplet ( $\mathbf{3}$ ) tetraquark, color-antitriplet ( $\bar{\mathbf{3}}$ ) diquark clusterization is the energetically most favorable configuration for a system with  $d'$  quantum numbers. For such a system, a relatively small mass of  $M_{d'} \approx 2100$  MeV has been obtained [23].

The six-quark wave function for the  $d'$  dibaryon is expanded into the  $\mathbf{3} \otimes \bar{\mathbf{3}}$  tetraquark-diquark cluster basis

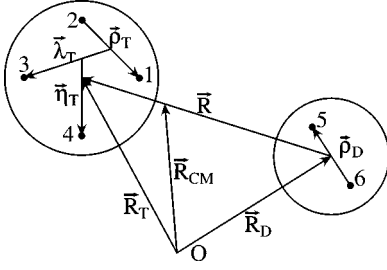


FIG. 4. The Jacobi coordinates in the  $q^2$ - $q^4$  colored cluster model of the  $d'$ .

$$\begin{aligned}
 |\Psi_{d'}^{J=0, T=0}\rangle = & \mathcal{A} \{ [\Phi_T^{S_T=1, T_T=0}(\boldsymbol{\rho}_T, \boldsymbol{\lambda}_T, \boldsymbol{\eta}_T) \times [211]_3^{C_T=1} \\
 & \otimes \Phi_D^{S_D=0, T_D=0}(\boldsymbol{\rho}_D) \times [11]_3^{C_D=\bar{1}}]^{S=1, T=0} \\
 & \otimes \chi_{L=1}(\mathbf{R}) \}^{J=0, T=0} [222]_1^{C=0}, \quad (13)
 \end{aligned}$$

where  $\Phi_T^{S_T=1, T_T=0}(\boldsymbol{\rho}_T, \boldsymbol{\lambda}_T, \boldsymbol{\eta}_T)$  and  $\Phi_D^{S_D=0, T_D=0}(\boldsymbol{\rho}_D)$  are the internal wave functions of the tetraquark ( $T$ ) and diquark ( $D$ ) clusters, respectively, and  $\chi_{L=1}(\mathbf{R})$  is the yet unknown relative wave function of the two colored clusters, projected onto good angular momentum  $L=1$ . The Jacobi coordinates introduced in Eq. (13) are depicted in Fig. 4. As usual in resonating group method (RGM) [45] calculations, ground-state  $s^2$  and  $s^4$  harmonic oscillator wave functions are used for the diquark and tetraquark clusters, respectively.

Equation (13) shows that the color triplet ( $\mathbf{3}$ ) tetraquark with mixed permutational symmetry  $[211]$ , and the color antitriplet ( $\bar{\mathbf{3}}$ ) diquark with permutational symmetry  $[11]$  is coupled to an overall color-singlet ( $\mathbf{1}$ ) six-quark state with mixed permutational symmetry  $[222]$  in color space. In contrast to mesons and baryons, the color state of a genuine  $q^6$  system is by itself not fully antisymmetric. There are both antisymmetric and symmetric quark pairs. Thus, in a compact  $q^6$  system, there is no factorization of the color space and the flavor-spin-orbital space, i.e., the color dynamics and the orbital structure of the system are correlated in a more complex manner [37]. This can be seen as an indication that the transition between  $q^3$  and compact  $q^6$  systems is not as trivial as usually assumed.

We recall that the stringlike bag model employs impenetrable diquark and tetraquark clusters, and the clusters cannot merge into a single bag. In contrast, an RGM calculation allows for a continuous transition from the compound  $q^6$  state, where all quarks are in a single potential well, to the  $q^2$ - $q^4$  clustered state, where one has two clearly separated bags. There is no artificial boundary between these extreme configurations, and they are both described by one and the same resonating group method wave function. Furthermore, the  $q^3$ - $q^3$  and  $q^5$ - $q^1$  partitioning into colored clusters, as well as the  $q^3$ - $q^3$  split into color-singlet clusters is automatically included in the present theory. These important properties are a consequence of the Pauli principle on the quark level which is ensured by the antisymmetrizer  $\mathcal{A}$

$$\mathcal{A} = 1 - 8P_{46}^{\text{OSTC}} + 6P_{35}^{\text{OSTC}}P_{46}^{\text{OSTC}}, \quad (14)$$

where  $P_{ij}^{\text{OSTC}}$  is the permutation operator of the  $i$ th and  $j$ th quark in orbital (O), spin-isospin (ST), and color space (C).

The direct, one-quark-, and two-quark-exchange contributions associated with the three terms in the antisymmetrizer of Eq. (14) are shown for the case of the one-gluon-exchange potential of Eq. (2) in Fig. 5.

The solution for the unknown relative wave function  $\chi_L(\mathbf{R})$  and the unknown eigenenergy  $E = M_{d'}$  is obtained from the Ritz variational principle

$$\delta \left[ \frac{\langle \Psi_{d'} | H - E | \Psi_{d'} \rangle}{\langle \Psi_{d'} | \Psi_{d'} \rangle} \right] = 0, \quad (15)$$

where the variation is performed with respect to the relative wave function  $\chi_L(\mathbf{R})$ . After expanding the relative motion wave function  $\chi_L(\mathbf{R})$  in a finite sum of Gaussians centered around the generator coordinates  $s_i$  [generator coordinate method (GCM)]

$$\begin{aligned}
 \chi_L(\mathbf{R}) = & \hat{P}_L \sum_i C_i \left( \frac{4}{3\pi b_6^2} \right)^{3/4} \exp \left( -\frac{2}{3} (\mathbf{R} - \mathbf{s}_i)^2 / b_6^2 \right) \Rightarrow |\Psi_{d'}\rangle \\
 = & : \mathcal{A} \sum_i C_i | \text{GCM}_i(\mathbf{s}_i) \rangle, \quad (16)
 \end{aligned}$$

and projecting onto good angular momentum  $L$  via  $\hat{P}_L \equiv 1/\sqrt{4\pi} \int d\hat{s}_i \cdot Y^L(\hat{s}_i)$  (cf. the Appendix for more details), Eq. (15) transforms into a generalized algebraic eigenvalue problem

$$\sum_i \mathcal{H}_{ij}(s_i, s_j) C_i = E \sum_i \mathcal{N}_{ij}(s_i, s_j) C_i. \quad (17)$$

The analytic expressions for the Hamiltonian kernel  $\mathcal{H}_{ij}(s_i, s_j) = \langle \text{GCM}_i | \mathcal{A} H | \text{GCM}_j \rangle$  and the norm kernel  $\mathcal{N}_{ij}(s_i, s_j) = \langle \text{GCM}_i | \mathcal{A} | \text{GCM}_j \rangle$  of Eq. (17) can be found in the Appendix. The norm matrix  $\mathcal{N}_{ij}(s_i, s_j)$  on the right-hand side of Eq. (17) reflects the nonorthogonality of the Gaussian basis functions in Eq. (16). For simplicity, and to avoid a proliferation of parameters, the same variational parameter  $b_6$  for the internal and relative motion wave functions of the six-quark system is used. This greatly facilitates the calculation of the norm and Hamiltonian integrals and restricts the variational space spanned by Eq. (16) only slightly.

Having solved the generalized eigenvalue problem, we determine the mass of the  $d'$  and the optimal harmonic oscillator parameter  $b_6$ , which plays the role of a nonlinear variational parameter, by minimization of the  $d'$  mass:

$$\partial E_{d'}(b_6) / \partial b_6 = 0. \quad (18)$$

We emphasize that the  $b_6$  values obtained in this way are some 20–30 % larger than the corresponding values  $b_3$  which minimize the nucleon mass. This observation is the basis for our conjecture that the two-body confinement strength in a compound six-quark system such as the  $d'$  is weaker than in a three-quark system (see Sec. IV C).

#### IV. RESULTS AND DISCUSSION

In this section we present the results of an RGM calculation for the mass and size of the  $d'$  dibaryon and compare it with the corresponding shell model and stretched-bag model

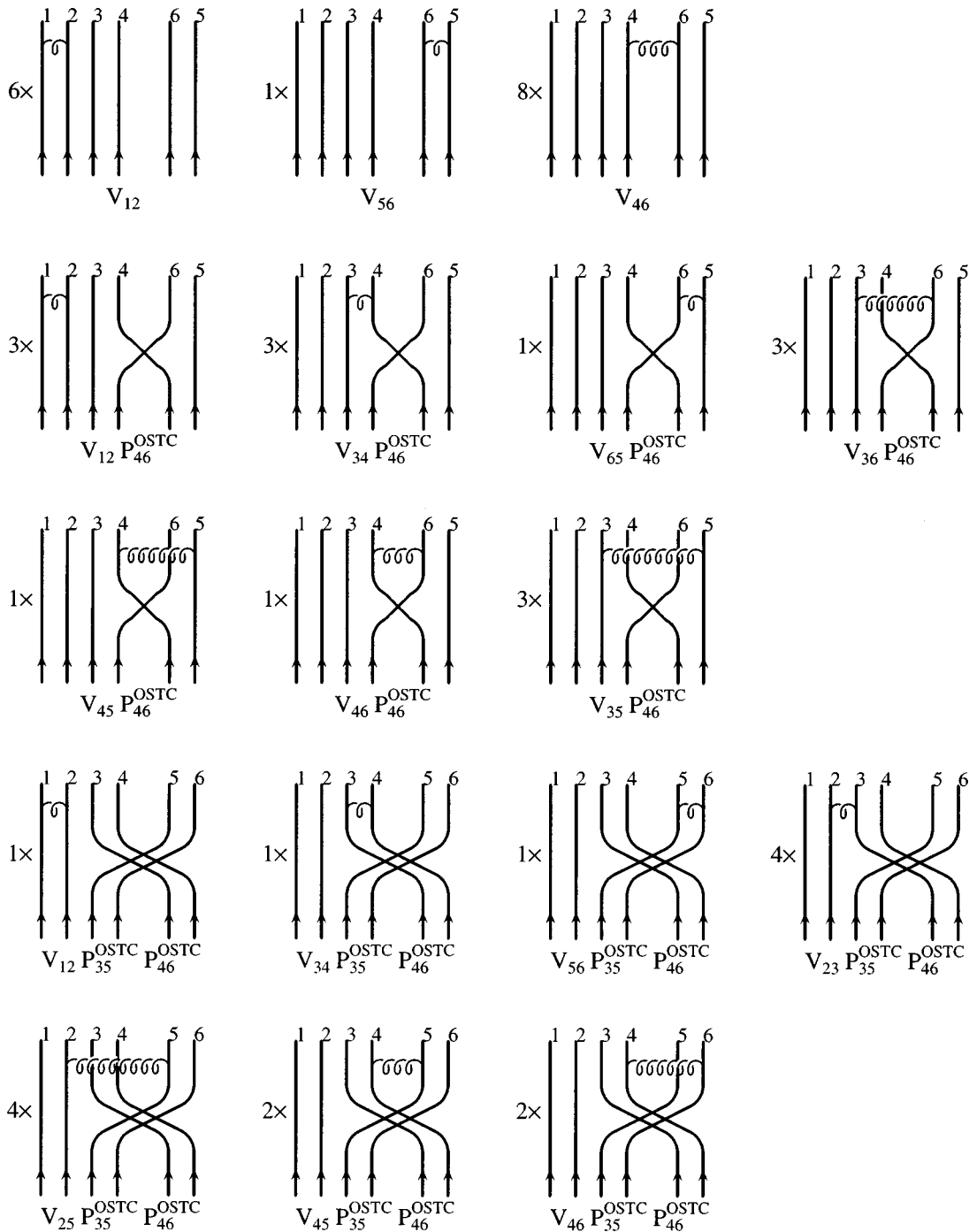


FIG. 5. The direct, one-quark  $V_{ij}P_{46}^{\text{OSTC}}$  and two-quark  $V_{ij}P_{46}^{\text{OSTC}}P_{35}^{\text{OSTC}}$  exchange diagrams for the one-gluon exchange potential. Corresponding diagrams are calculated for the confinement, one-pion, and one- $\sigma$  exchange potentials. The stringlike bag model includes only the diagrams in the first row. The quark exchange diagrams necessary to satisfy the Pauli principle for the whole six-quark system are neglected in the stringlike bag model but included in the present theory. The quark exchange kernels *increase* the  $d'$  mass by about 100 MeV.

results [46]. Because a corresponding RGM calculation for the deuteron, based on the same Hamiltonian and colorless nucleon cluster wave functions accurately reproduces the deuteron energy and wave function [14], we are confident that the absolute mass scale of our predictions is correct, and the calculated  $d'$  masses are reliable.

#### A. Mass of the $d'$

The mass of the  $d'$  is obtained as the lowest eigenvalue  $E$  of the bound-state GCM equation (17), and by subsequent

optimization with respect to  $b_6$  according to Eq. (18). It is interesting to isolate the effect of the Pauli principle on the mass of the  $d'$  by performing a calculation where the quark exchange kernels have been turned off, i.e., only the first term in the antisymmetrizer of Eq. (14) is taken into account, before solving Eq. (17). We use the same  $b_6$  as in the full calculation including all exchange kernels. Results for  $M_{d'}$  and  $b_6$  are shown in Table II for the parameter sets of Table I. A comparison of the results for the  $d'$  mass with and without quark exchange show that the quark exchange inter-

TABLE II. The mass  $M_{d'}$  and characteristic size  $b_6$  of the  $d'$  as obtained according to Eq. (18) for the six parameter sets of Table I. The diquark and tetraquark masses are also shown. The masses in the last column are obtained in a calculation without quark exchange between the diquark and the tetraquark clusters. As in Table I, the abbreviations  $Q$ ,  $L$ ,  $R$ , and  $E$  identify the four different confinement models used in this work. The experimental mass of the  $d'$  is  $M_{d'} = 2065 \pm 5$  MeV [3].

Conf.	Set	$M_{2q}$ (MeV)	$M_{4q}$ (MeV)	$M_{d'}$ (MeV)	$b_6$ (fm)	$M_{\text{no QEX}}$ (MeV)
$Q$	I	636	1501	2610	0.70	2490
$Q$	II	643	1456	2440	0.75	2316
$Q$	III	621	1309	2092	0.95	2013
$L$	IV	650	1431	2354	0.86	2261
$R$	V	653	1419	2313	0.93	2234
$E$	VI	661	1422	2288	1.08	2235

actions contribute an additional energy of 50–120 MeV depending on the model of confinement (see sets I–VI in Table II).

We note that the  $d'$  mass calculated with model I (quadratic confinement and one-gluon exchange) is some 550 MeV above the experimental mass of the  $d'$ . An RGM calculation without  $\pi$ - and  $\sigma$ -meson exchange forces in the Hamiltonian, but with a  $q^3$ - $q^3$  clusterization of the quarks has already been performed many years ago [47]. The quark-quark interaction of Ref. [47] is very similar to model I, and the method of fitting the quark model parameters to single-baryon properties is the same as in the present work. Although the authors of Ref. [47] use two color-octet three-quark clusters, i.e.,  $(\mathbf{8} \otimes \mathbf{8})^1$  whereas we use color-(anti)triplet diquark and tetraquark clusters, i.e.,  $(\bar{\mathbf{3}} \otimes \mathbf{3})^1$ , it is nevertheless meaningful to compare their results and our results.

Due to the quark antisymmetrizer  $\mathcal{A}$  of Eq. (14) acting on all six quarks, the three different arrangements of the six-quarks into *colored* clusters, namely  $q^3$ - $q^3$ ,  $q^2$ - $q^4$ , and  $q^1$ - $q^5$  are approximately equivalent for the relevant intercluster distances involved. In fact, in the region of complete cluster overlap, that is, in the limit for  $s_i = s_j \rightarrow 0$  all three partitions have the same six-quark shell-model limit, i.e., the unique  $s^5 p^1$  TISM state. Thus, by virtue of the antisymmetrizer, the RGM wave function not only contains the  $(\bar{\mathbf{3}} \otimes \mathbf{3})^1$  component, but also the  $(\mathbf{8} \otimes \mathbf{8})^1$  component. It is reassuring that the results of Ref. [47]  $M_{d'} = 2540$  MeV, and of the present work  $M_{d'} = 2610$  MeV (see set I in Table II) are in very good agreement. However, both are  $\sim 500$  MeV above the experimental resonance position. Before drawing any conclusions concerning the existence of the  $d'$ , we first study how these results depend on the choice of the quark-quark interaction.

In model II, we use the full Hamiltonian including one-gluon exchange,  $\pi$ - and  $\sigma$ -exchange [50], and a quadratic confinement potential between the constituent quarks. The inclusion of the chiral  $\pi$ - and  $\sigma$ -exchange interactions reduces the  $d'$  mass by 160 MeV compared to model I. It is, however, with 2440 MeV still about 380 MeV higher than the experimental value.

Model III is very different from all other confinement models. It uses a different confinement strength for the three-quark (nucleon) and the six-quark system ( $d'$ ) and leads to a  $d'$  mass close to the experimental result. Before we try to justify this apparently *ad hoc* step, we study the dependence of the  $d'$  mass on the radial form of the confinement potentials given by Eqs. (8)–(10) and shown in Fig. 3.

The slope of models (IV–V) is for  $r \geq 1$  fm considerably flatter than that of the quadratic confinement of Eq. (7). For these potentials, the stability condition Eq. (18) leads to larger oscillator parameters  $b_6$  (larger dibaryons), which in turn results in a reduction of the kinetic energy and the  $d'$  mass. For example, the linear confinement potential (model IV) reduces the  $d'$  mass by about 90 MeV in comparison to the quadratic confinement (model II). For the  $r^{2/3}$  confinement (model V), the corresponding reduction is 130 MeV.

Model VI, the color-screened error-function confinement, displays a qualitatively different behavior at small and large interquark distances. At short distances, it is approximately linear and at larger distances it goes to a constant. While baryons feel mainly the linear rising part, dibaryons are due to their larger size also very sensitive to the long-range tail of the confinement potential. The screening of color charges at larger interquark distances leads to a reduction of the  $d'$  mass by 150 MeV compared to the quadratic confinement (model II) and also to a larger value for the oscillator parameter  $b_6$ .<sup>1</sup> However, the  $d'$  mass is with 2288 MeV still some 220 MeV above the experimental value of  $M_{d'}^{\text{exp}} = 2065$  MeV. If we use the  $1 - \exp(-\mu r^2)$  color-screening model of Ref. [42] with  $\mu = 1 \text{ fm}^{-2}$  for all quark pairs in the system, we obtain  $M_{d'} = 2468$  MeV at  $b_6 = 0.82$  fm. In this context, we mention that at interquark distances corresponding to 3–4 times the screening length  $1/\mu = 0.8$  fm, the effective confinement force  $-\partial V_{\text{eff}}^{\text{conf}}(r)/\partial r$  between the colored clusters tends quickly to zero. The stability of the system is nevertheless preserved due to Eq. (18) and our use of Gaussian trial wave functions. Model VI represents a limiting confinement model especially for dibaryons, and we expect that the  $d'$  mass cannot be further reduced by an significant amount by considering another radial form of the confinement potential.

In Table III we list the individual contributions of the kinetic, confinement, one-gluon-, one-pion-, and one- $\sigma$ -exchange potentials to the  $d'$  mass for the different confinement models. The results in parentheses give the corresponding contributions without the quark exchange diagrams. One observes a drastic reduction of the kinetic energy for the larger dibaryon systems. We also see that the dominant attraction is due to the color-Coulomb part of the interaction.

Thus, we observe a clear trend when going from a quadratic (model II) to a color-screened confinement model (VI): The slower the increase of the confinement potential at larger  $r$ , the larger the size  $b_6$ , and the smaller the mass of the  $d'$ . However, even for the limiting case of the color-

<sup>1</sup>In the suggested range for the color-screening length  $0.8 \text{ fm} < 1/\mu < 1.2 \text{ fm}$  [41], our results are not very sensitive to the actual value of  $1/\mu$ .

TABLE III. The kinetic (without rest masses) and potential energy contributions to the mass  $M_{d'}$  of the  $d'$  for the six parameter sets of Table I. The numbers in parentheses are obtained in a calculation without quark exchange between the diquark and the tetraquark clusters.

Conf.	Set	$E_{\text{kin}}$ (MeV)	$V_{\text{conf}}$ (MeV)	$V_{\text{gluon}}$ (MeV)	$V_{\pi}$ (MeV)	$V_{\sigma}$ (MeV)	$M_{d'}$ (MeV)
$Q$	I	1048 (997)	725 (678)	-1041 (-1063)			2610 (2490)
$Q$	II	906 (866)	460 (429)	-617 (-634)	-44 (-86)	-143 (-137)	2440 (2316)
$Q$	III	566 (545)	270 (249)	-517 (-537)	-23 (-42)	-82 (-79)	2092 (2013)
$L$	IV	677 (651)	547 (524)	-615 (-636)	-32 (-57)	-101 (-98)	2354 (2261)
$R$	V	574 (554)	580 (562)	-610 (-634)	-27 (-45)	-82 (-81)	2313 (2234)
$E$	VI	396 (402)	722 (719)	-639 (-682)	-21 (-28)	-49 (-54)	2288 (2235)

screened confinement potential, the results for the  $d'$  mass are 220 MeV above the empirical  $d'$  mass. We conclude that in the present constituent quark model framework, a change in the radial form of the confinement potential is insufficient to generate a  $d'$  dibaryon with a mass of 2065 MeV.

### B. Wave function and size of the $d'$

We turn now to the discussion of the relative wave function as obtained from eigenvalue equation (17) and the radius of the  $d'$ . Figure 6 shows the wave function  $\chi_{L=1}(R)$  for the two extreme confinement models II and VI, using the same Hamiltonian as in the three-quark sector. The RGM wave function is calculated both with (Pauli-on) and without (Pauli-off) the quark exchange diagrams. For the quadratic confinement model II, one observes that the relative wave function has already died out at intercluster distances of about 2.5 fm, while for confinement model VI it still has an appreciable amplitude even at 4 fm. The quark exchange diagrams lead for model II to an additional attraction between the two colored clusters, as reflected by the smaller radial extension of the relative wave function, while they are rather unimportant for model VI.

A quantitative measure of the extension of the relative cluster wave function is the root-mean-square (rms) distance,  $R_{d'}^{\text{RGM}}$ , which measures the mean distance between the  $q^2$  and  $q^4$  clusters

$$(R_{d'}^{\text{RGM}})^2 = \frac{\langle \chi_{L=1}(R) | R^2 | \chi_{L=1}(R) \rangle}{\langle \chi_{L=1}(R) | \chi_{L=1}(R) \rangle}. \quad (19)$$

Here,  $R$  is the relative coordinate connecting the centers of the two clusters. This distance corresponds to the length  $l$  of the color flux tube in the stringlike bag model.

The rms distance of Eq. (19) does not yet take into account the finite size of the clusters. In the present model these are given as

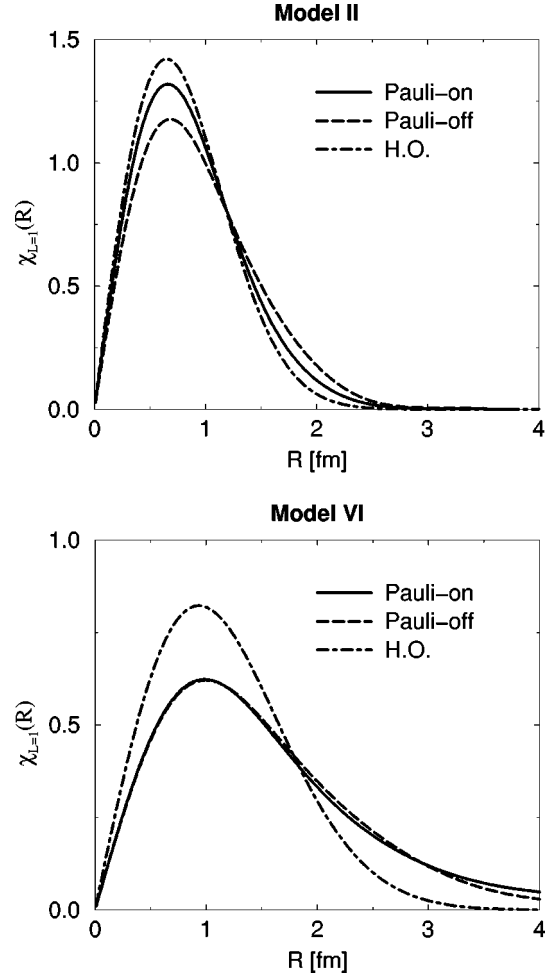


FIG. 6. The relative wave RGM function between the tetraquark and diquark clusters with (Pauli-on) and without (Pauli-off) inclusion of the quark exchange diagrams for the smallest (model II) and largest (model VI)  $d'$  dibaryon. The RGM wave functions are compared to the pure harmonic-oscillator wave function of Eq. (23). The upper graph shows the results for the quadratic confinement (model II), while the lower graph is obtained for the color-screened confinement (model VI). For model II (upper graph) the clusters overlap, while they are just touching in model VI. The corresponding rms radii are given in Table IV. The wave functions of the other models are in between these two extremes.

$$r_D^2 = \left\langle \Phi_D \left| \frac{1}{2} \sum_{i=1}^2 (\mathbf{r}_i - \mathbf{R}_D)^2 \right| \Phi_D \right\rangle = \frac{3}{4} b^2;$$

$$r_T^2 = \left\langle \Phi_T \left| \frac{1}{4} \sum_{i=1}^4 (\mathbf{r}_i - \mathbf{R}_T)^2 \right| \Phi_T \right\rangle = \frac{9}{8} b^2. \quad (20)$$

Here,  $\mathbf{R}_D$  and  $\mathbf{R}_T$  are the center-of-mass coordinates of the diquark and tetraquark, respectively. One then finds for the total  $d'$  radius in the RGM formalism

$$r_{d'}^2 = r_D^2 + r_T^2 + \left( \frac{1}{2} R_{d'}^{\text{RGM}} \right)^2 + r_q^2, \quad (21)$$

where the last term is due to the finite size of the constituent quark. In Table IV, the radii of the diquark, tetraquark, and the relative cluster wave function,  $R_{d'}^{\text{RGM}}$ , are shown for dif-

TABLE IV. The rms radii of the diquark ( $r_D$ ), tetraquark ( $r_T$ ), and the intercluster wave function ( $R_{d'}^{\text{RGM}}$ ) with and without (in parentheses) the quark exchange diagrams. The total  $d'$  matter radius  $r_{d'}$  [see Eq. (21)] is also given. In the RGM formalism the same value for the oscillator parameter ( $b_6$ ) is used for the diquark, tetraquark, and relative motion wave functions. The mean distance between the colored clusters,  $R_{d'}^{\text{RGM}}$ , is compared to the corresponding shell-model radius  $R_{d'}^{\text{HO}} = (15/8)b_6^2$ . The mean distance between two quarks in the RGM ( $r_{qq}^{\text{RGM}}$ ) and TISM ( $r_{qq}^{\text{TISM}}$ ) approach are also shown for comparison. The same notation as in Table I is used.

Conf.	Set	$r_D$ (fm)	$r_T$ (fm)	$R_{d'}^{\text{RGM}}$ (fm)	$r_{d'}$ (fm)	$R_{d'}^{\text{HO}}$ (fm)	$r_{qq}^{\text{RGM}}$ (fm)	$r_{qq}^{\text{TISM}}$ (fm)
$Q$	I	0.61	0.74	1.01 (1.11)	1.16	0.96	1.32	1.38
$Q$	II	0.65	0.80	1.10 (1.21)	1.24	1.03	1.42	1.47
$Q$	III	0.82	1.01	1.39 (1.50)	1.53	1.30	1.80	1.82
$L$	IV	0.74	0.91	1.32 (1.43)	1.41	1.18	1.67	1.73
$R$	V	0.81	0.99	1.46 (1.56)	1.53	1.27	1.84	1.86
$E$	VI	0.93	1.15	2.08 (1.94)	1.85	1.48	2.52	2.25

ferent confinement potentials. Neglecting quark exchange between clusters increases  $R_{d'}^{\text{RGM}}$  typically by about 10% (numbers in parentheses). This shows that the quark exchange matrix elements provide additional color attraction. Depending on the confinement model, the rms distances  $R_{d'}^{\text{RGM}}$  lie between 1.0 and 2.0 fm, while the corresponding tetraquark radii  $r_T$  vary between 0.74 and 1.15 fm.

In order to have another measure of the size of the  $d'$ , we calculate the rms distance between an arbitrary pair of quarks in the dibaryon<sup>2</sup>

$$(r_{qq}^{\text{RGM}})^2 = \left\langle \Psi_{d'} \left| \frac{1}{N_{\text{pairs}} \sum_{i < j}^6} (\mathbf{r}_i - \mathbf{r}_j)^2 \right| \Psi_{d'} \right\rangle, \quad (22)$$

where  $N_{\text{pairs}} = 15$  is the number of quark pairs in a six-quark system. The spatial extension of the quark distribution in the  $d'$  is close to the value given by Eq. (22). The radius defined in Eq. (22) facilitates the comparison with the shell-model description of the  $d'$  [26,27,46]. The numerical results for  $r_{qq}^{\text{RGM}}$  are given in the second to last column of Table IV.

### 1. Comparison with the six-quark shell model

In Fig. 6 we also compare the  $q^2 - q^4$  relative RGM wave function with an unperturbed six-quark  $1\hbar\omega$  ( $s^5p^1$ ) harmonic-oscillator wave function

$$\chi_{L=1}^{s^5p^1}(R) = \frac{16}{3\sqrt{3}\sqrt{3\pi}b_6^5} R \exp\left(-\frac{2}{3} \frac{R^2}{b_6^2}\right), \quad (23)$$

<sup>2</sup>Note that in the case of the nucleon the mean distance between any pair of quarks is  $b_3 \cdot \sqrt{3} \approx 1$  fm.

with the same oscillator parameter  $b_6$ . Our previous results [27] using the translationally invariant shell model (TISM) have shown that admixtures of excited shell-model states to the unique lowest-lying  $s^5p^1$ ,  $1\hbar\omega$  shell-model state of Eq. (23) are small.

For the quadratic confinement model II, the  $d'$  wave function does not display a pronounced clusterization but resembles rather closely the six-quark harmonic oscillator wave function of Eq. (23). The agreement between the pure harmonic oscillator wave function and the RGM wave function is more complete when the quark exchange diagrams are included. On the other hand, the RGM wave function of model VI extends to larger intercluster distances  $R$  than the unperturbed shell-model state of Eq. (23). This is a consequence of the color-screened confinement potential, which provides only weak confinement forces at large interquark distances. In order to describe the long-range RGM wave function in the shell model, one would need substantial admixtures of excited harmonic-oscillator states. As one might expect, the effect of the quark exchange diagrams on the wave function is here much smaller than for the quadratic confinement case, which can also be seen from Table II.

For the wave function of Eq. (23), the mean-square (ms) distance between the clusters is given by

$$(R_{d'}^{\text{HO}})^2 = \langle \chi_{L=1}^{s^5p^1} | R^2 | \chi_{L=1}^{s^5p^1} \rangle = \frac{15}{8} b_6^2. \quad (24)$$

For all but one model, the rms distance between the  $q^2$  and  $q^4$  clusters as calculated in RGM is slightly larger than the corresponding quantity in the harmonic-oscillator model. Only in the case of the color-screened confinement potential (model VI), we find a pronounced increase of  $R_{d'}^{\text{RGM}}$  by 40% compared to  $R_{d'}^{\text{HO}}$ , indicating that the system is partially clusterized.

In the case of the TISM wave function including shell-model configurations up to  $3\hbar\omega$  [27], the rms distance between any two quarks in the  $d'$  is given by

$$(r_{qq}^{\text{TISM}})^2 = b_6^2 \left( \frac{17}{5} + (1 - \alpha^2) \frac{4}{5} \right), \quad (25)$$

where  $\alpha^2$  denotes the probability of finding the (unique) energetically lowest-lying  $N=1$  shell-model configuration in the total TISM wave function of the  $d'$ . The values given in Table IV are obtained for a harmonic-oscillator parameter  $b_6$ , which minimizes the  $d'$  mass in the RGM (see Table II), or TISM approach (last column).

For models I–V, the rms distance between an arbitrary pair of quarks  $r_{qq}^{\text{RGM}}$  follows closely the corresponding TISM result  $r_{qq}^{\text{TISM}}$ . Only for the color-screened confinement (set VI), the average distance between quarks in the cluster model  $r_{qq}^{\text{RGM}}$  is increased by about 10% with respect to the corresponding shell-model result  $r_{qq}^{\text{TISM}}$ . This is mainly due to the *intercluster* quark pairs, which due to the screening are preferably at larger relative distances.

Thus, a comparison of the cluster model and shell-model results [27] reveals an overall agreement for the orbital structure and size of the  $d'$ . In addition, the two calculations agree also for the individual kinetic and different potential

energy contributions to the  $d'$  mass (as given for the cluster model in Table III), and thus also for the  $d'$  mass itself. The agreement is quantitative for models I–V. However, the longer tail of the RGM wave function of model VI shown in Fig. 6 and the larger rms radius listed in Table IV show that certain confinement models lead to deviations from a pure  $s^5p^1$  shell-model structure and favor a clusterization of the quarks into colored quark clusters.

Let us briefly discuss the reasons for the quantitative agreement between the two structurally quite different calculations. The outer product of the  $[4]_O$  (tetraquark) and  $[2]_O$  (diquark) orbital symmetries ( $s^4$  and  $s^2$ ) gives according to Littlewood's theorem the following  $S_6$  permutational symmetries in orbital space

$$[4]_O \otimes [2]_O = [42]_O \oplus [51]_O \oplus [6]_O. \quad (26)$$

For  $d'$  quantum numbers, the fully symmetric  $[6]_O$  orbital symmetry, corresponds to a spurious center of mass excitation of the six-quark state, and is automatically excluded in both approaches. The orbital symmetries  $[51]_O$  and  $[42]_O$  in Eq. (26) are also included in the enlarged  $N=3\hbar\omega$  shell-model basis [27]. Analogously, the outer product of the two clusters in spin-isospin space leads to

$$[31]_{ST} \otimes [2]_{ST} = [51]_{ST} \oplus [42]_{ST} \oplus [33]_{ST} \oplus [411]_{ST} \\ \oplus [321]_{ST}. \quad (27)$$

Comparison with Eq. (10) in our previous TISM calculation [26] shows that the  $q^2-q^4$  cluster model wave function comprises the same  $S_6$  symmetries in spin-isospin space (with the exception of the  $[2211]_{ST}$  symmetry which does not appear in the cluster model) as the enlarged shell-model basis. Thus the trial function space spanned by both sets of basis functions is nearly equivalent.

## 2. Comparison with the stringlike bag model

It is interesting to compare the description of the  $d'$  in the cluster model with the one in the stringlike bag model. With respect to the sizes, the cluster model values  $R_{d'}^{\text{RGM}}$  and  $r_T$  have to be compared to the length  $l$  and radius  $R_0$  of the color flux tube in the stringlike bag model. In the stretched-bag model [23], the radius  $R_0$  and length  $l$  of the flux tube are given as

$$R_0 = \sqrt{\frac{\alpha}{24\pi B}}, \quad l = \frac{M_{d'}}{4\pi B R_0^2},$$

respectively, where  $\alpha = 1.1 \text{ GeV}^2$  is the ‘‘universal’’ string tension,  $B = 59 \text{ MeV fm}^{-3}$  the bag constant, and  $M_{d'} = 2100 \text{ MeV}$  is the mass of the resonance. One then obtains for the ‘‘universal’’ radius of the color flux tube  $R_0 = 1.1 \text{ fm}$  and  $l = 2.3 \text{ fm}$  [23].

According to Ref. [23], the stretched-bag model is only valid if  $l > 2R_0$ , and for a low-lying resonance of  $M_{d'} = 2100 \text{ MeV}$  this condition is barely satisfied. If we now identify the bag model quantities  $l$  and  $R_0$  with the cluster model quantities  $R_{d'}^{\text{RGM}}$  and  $r_T$ , respectively, we see that this condition is generally not satisfied in the present calculation. In fact, from Table IV it is evident, that the sum of the

cluster radii exceeds the intercluster radius by about half the diquark radius. This means that there is considerable overlap between the clusters. Only for the color-screened confinement potential, we observe a modest clusterization that is, however, insufficient to justify a stringlike bag model treatment.

At this point, we comment on the universality of the string tension  $\alpha$  in the stringlike bag model [23], which predicts a series of orbitally excited meson, baryon, and dibaryon states with orbital angular momentum  $L$ , and with masses given by

$$M^2 = \alpha L + M_0^2. \quad (28)$$

The mass of the clusters at the ends of the string,  $M_0$ , is calculated in the *spherical* bag model, and  $\alpha$  is the common string tension for mesons ( $q-\bar{q}$ ), baryons ( $q^1-q^2$ ), and dibaryons ( $q^4-q^2$ ) which is given by

$$\alpha = \sqrt{8\pi B} \alpha_s f_C^2, \quad (29)$$

where  $B$  is the bag constant determining the constant color-electric-field strength  $\mathbf{E}$  in the string,  $\alpha_s$  is the quark-gluon coupling, and  $f_C^2$  is the eigenvalue of the quadratic Casimir operator of  $\text{SU}(3)_{\text{color}}$  in a given color representation. It is important to recall that the string tension  $\alpha$  and the related transverse radius of the string  $R_0$  are defined only for well separated clusters with sufficiently high relative angular momentum  $L$  [23].

A universal string tension  $\alpha$  results because it is *assumed* that the individual clusters are so far apart that they are always in the color-triplet  $\mathbf{3}$  or color-antitriplet  $\bar{\mathbf{3}}$  representation, for which the Casimir operator has the common eigenvalue  $f_C^2 = 4/3$ . In this case, there is only one type of color string with a unique string tension given by Eq. (29). Obviously, this assumption is justified as long as the clusters do not overlap. However, we have seen that for most confinement models there is considerable overlap between the colored diquark and tetraquark clusters. Consequently, the tunneling of quarks from one cluster to the other can change the color-representation (e.g., into  $\mathbf{8} \otimes \bar{\mathbf{8}}$ , or  $\mathbf{6} \otimes \bar{\mathbf{6}}$ ) of the clusters and therefore also the string tension. For the octet and sextet color representations, which are not present in mesons and baryons, one has  $f_C^2 = 3$  and  $f_C^2 = 10/3$ , respectively. Thus, one obtains a stronger string tension in both cases. The authors of Ref. [23] only include the energetically most favorable case of a  $\mathbf{3} \otimes \bar{\mathbf{3}}$  string. If the Pauli principle is to be rigorously satisfied in Ref. [23] also the  $\mathbf{6} \otimes \bar{\mathbf{6}}$  and the  $\mathbf{8} \otimes \bar{\mathbf{8}}$  color configurations would have to be admixed and the corresponding  $d'$  mass would come out higher. This qualitatively agrees with our results for the  $d'$  mass (see Tables II and III) which are increased by the quark exchange interactions.

There is another difference between the present RGM calculation and the stringlike bag model. For the meson ( $q-\bar{q}$ ), baryon ( $q-q^2$ ), and dibaryon ( $q^4-q^2$ ) resonances, the sizes of the color sources (clusters) and therefore the transverse radii of the flux tubes are in reality rather different. A tetraquark in a dibaryon has a larger radius than a single quark in a baryon. Although a tetraquark and a single

quark carry the same color charge, the energy density of the color electric field,  $E^2/2$ , in the neighborhood of an extended tetraquark is smaller than in the neighborhood of a single quark. This difference is rather important for low angular momentum states. In the stretched-bag model, the energy density of the string is given by the bag constant  $B$ . A decrease of the energy density of the string for  $q^4 - q^2$  dibaryons compared to  $q - q^2$  baryons is related to a decrease of the effective bag constant  $B$ .<sup>3</sup> According to Eq. (29) this leads to a reduced effective string tension for dibaryons. This reduction of the string tension clearly outweighs its increase due to quark exchange.

In conclusion, the assumption of a universal string tension is *not* justified for *ground states*, such as the pion, nucleon, or the  $d'$  dibaryon. We emphasize once again that the string-like bag model is valid only for *higher* angular momentum states, where the clusters are well separated due to the centrifugal barrier, and where the tunneling of quarks, as well as the size difference of the color sources can be neglected.

### C. The $d'$ as an indication for a weaker confinement strength in a compound six-quark system?

So far we have studied how different confinement models affect the mass and characteristic size of the dibaryon. In all cases, we obtained dibaryon masses some 200–400 MeV above the experimental value. We point out that up to this point, we have used the same parameters as previously determined from the properties of color-singlet baryons [see Eq. (12)]. Although it is reasonable to expect such a universality of parameters for the microscopically better founded gluon-, pion- and  $\sigma$ -exchange interactions, the assumption that the confinement strength remains unmodified when going from a three-quark to a six-quark system is most likely too restrictive.

At present, there is no commonly accepted theory of color confinement. Different models of confinement have a limited range of validity. From the experimental information on the excited nucleon spectrum, combined with certain assumptions concerning the Lorentz structure, radial form, and color dependence, phenomenologically successful confinement models for baryons have been constructed. However, it is not at all obvious that one can extrapolate the experience gathered in the color-singlet three-quark sector to compound six-quark systems. We recall that the confinement strength  $a_c$  is usually determined from the experimental level spacing  $\omega$  between excited single-baryon states. Unfortunately, there is hardly any three-star data on excited six-quark resonances that would shed light on the confinement dynamics in a six-quark system.

We have seen that in the  $d'$ , the average distance between any two quarks is somewhat larger than in the nucleon. Consequently, the  $d'$  tests the confinement interaction at larger quark-quark distances where new physical phenomena come into play. For example, at large interquark distances, quark-antiquark pair creation [41,42] leads to a screening of the original color charges. This color-screening effect can be

simulated by a reduced effective confinement strength in the six-quark system as compared to the three-quark system.

Although we do not know how to calculate the effective confinement strength for three- and compound six-quarks systems from first principles, we can gain some qualitative understanding of the changing confinement dynamics using the harmonic-oscillator model. If the effective quark-quark interaction were a pure harmonic-oscillator confinement force, there would be an inverse proportionality between the confinement strength  $a_c^{(N)}$

$$a_c^{(N)} = \frac{1}{2m_q b_{(N)}^4 N} \quad (30)$$

and the fourth power of the harmonic-oscillator parameter  $b_{(N)}$ .

In model II, we have used one and the same two-body confinement strength for three-quark and six-quark systems in the numerical calculation, *even though the variational principle of Eqs. (12) and (18) tells us that the characteristic sizes of the  $d'$  ( $b_6$ ) are about 30% larger than those of the nucleon ( $b_3$ )*. Thus, in a model where the two-body harmonic-oscillator confinement is the only quark-quark interaction, there is a unique relation between the two-body harmonic confinement strength and the size of the system. We take this observation as the basis for our conjecture that the *effective* two-body confinement strength could be weaker than in a three-quark system [46]. Although the actual dependence of the effective confinement strength on the size of the system may be somewhat different for more realistic confinement models, we expect that an inverse proportionality between the confinement strength and the size of the system remains.

Model III differs from model II only in the strength of the parameter  $a_c^{(6)}$ , for which we have taken the value  $a_c^{(6)} = 5.0 \text{ MeV/fm}^2 \approx a_c^{(3)}/3$  [53]. All other parameters in the Hamiltonian are identical to the ones of model II. The proposed weaker two-body confinement in a six-quark system leads to a larger  $d'$  and a mass that is close to the experimental  $d'$  mass. Conversely, one could take the empirical  $d'$  mass as evidence for a weaker *effective* two-body confinement strength in a compound six-quark system because in the present model this is the only way to obtain the  $d'$  resonance mass, which is needed to fit the DCX data.

### D. Two-baryon vs six-quark description of dibaryons

The use of a reduced confinement strength in a compound six-quark system, where all quarks are basically in a single bag, is presumably not in conflict with our previous results for the deuteron. The deuteron is well described by an RGM wave function that is built from two colorless three-quark clusters. The contribution of compound six-quark states to the deuteron wave function is rather small.

Here, we would like to contrast the description of the  $d'$  dibaryon as a compound six-quark state with the successful picture (in terms of quarks) of the deuteron as a bound system of two color-singlet objects. This comparison clearly shows that the orbital structure of these systems is determined by an interplay of the Pauli principle and different parts of the effective quark-quark interaction.

<sup>3</sup>The universality of the bag constant for baryons and dibaryons has been questioned before [48].

It has been known for more than a decade that quark exchange between nucleons (Pauli principle) together with the spin-dependent quark-quark interactions provide an effective short-range repulsion in the  $NN$  system [54]. The latter prevents appreciable cluster overlap and is therefore mainly responsible for the successful description of the deuteron as a system of two colorless nucleons with an average distance of about 4 fm between the nucleons. To explain this in terms of a six-quark shell model we form the outer product of two  $s^3$  nucleons. One then obtains the following spatial permutational symmetries of a six-quark system:

$$[3]_o \otimes [3]_o = [6]_o \oplus [42]_o \oplus [51]_o \oplus [33]_o.$$

In a six-quark system with even orbital angular momentum, only the  $[6]_o$  and  $[42]_o$  symmetries occur. The important role of the orbital  $[42]_o$  symmetry for the short-range repulsion in the  $NN$  system has been elucidated in Ref. [54]. In the shell model, which is appropriate for short  $NN$  distances, the short-range repulsion is achieved through a destructive interference of the excited  $s^4p^2$  six-quark state and the  $s^6$  six-quark state. The spin-dependent quark-quark interactions lower the energy of the excited  $s^4p^2$  state and raise the energy of the  $s^6$  state. As a consequence, the excited  $s^4p^2$  state is admixed with equal weight but with opposite sign to the  $s^6$  ground state so that it interferes destructively. This in turn leads to an almost complete cancellation of the wave function in the region of cluster overlap and consequently to the suppression of the deuteron wave function at short distances [55]. Furthermore, explicit calculation shows that the deuteron wave function is insensitive to the details of the confinement mechanism.

On the other hand, in the case of the  $NN$ -decoupled  $d'$  dibaryon, the radial form of the confinement potential crucially affects the mass and wave function of the system as we have demonstrated. The spin-dependent interactions are of minor importance. The latter point is reflected by the small admixtures of excited states to the lowest-lying  $s^5p^1$  shell-model state. Because the Pauli principle prevents a clusterization of the six quarks into two colorless nucleons, the energetically lowest configuration is a compound six-quark state. Thus, for both, the deuteron and the  $d'$ , the Pauli principle determines whether the residual spin-dependent or the confining interactions prevail, and hence determines the orbital structure of the system.

## V. SUMMARY

In the present work, we have calculated the mass and wave function of a  $J^P=0^-, T=0$  six-quark system, called  $d'$ , in a colored diquark-tetraquark cluster model using the resonating group method (RGM). This method determines the orbital configuration of the six-quark system dynamically, i.e., according to the given Hamiltonian. Thus we may test the validity of the assumption that the  $d'$  is a stretched diquark-tetraquark system. In contrast to the stringlike bag model, which employs a single nonantisymmetrized  $q^2-q^4$  dumbbell-like configuration, the present RGM calculation also includes other clusterizations, such as the  $q^1-q^5$ ,  $q^3-q^3$  and the single  $q^6$  state. This remarkable property is a consequence of the proper antisymmetrization of the total

six-quark RGM wave function.

A major purpose of this work has been to study the effect of quark exchange interactions between the colored clusters on the mass and wave function of the  $d'$ . The quark exchange interactions between the colored diquark and tetraquark clusters *increase* the  $d'$  mass by some 100 MeV and slightly decrease the size of the  $d'$  compared to a calculation without quark exchange. Our results for the  $d'$  mass and wave function are rather similar to a previous six-quark shell-model calculation [26,27,46]. This means that for confinement models I–V, the  $d'$  is in reality not a clusterized  $q^4-q^2$  state, but better described as a single six-quark  $s^5p^1$  shell-model state, where all quarks move in a common potential well. For this conclusion, it is crucial that the quark exchange diagrams are included in the cluster model.

In order to investigate how our results depend on the model of confinement, we have studied various, commonly used confinement potentials. All models yield  $d'$  masses substantially larger than the empirical value. Depending on the confinement model we obtain  $d'$  masses that lie roughly 200–400 MeV above the experimentally required resonance energy of  $M_{d'}=2065$  MeV. Thus, we conclude that irrespective of the radial form of the confinement potential, we cannot describe a  $J^P=0^- T=0$  dibaryon with a mass of 2065 MeV if we use the same confinement strength as in a three-quark system. Can one conclude that the  $d'$  does not exist?

In a six-quark system, such as the  $d'$ , the confinement interaction is tested in a heretofore unexplored regime where new physical phenomena, such as color-screening due to quark pair creation and many-body confinement forces, are expected to play an important role. These long-range effects are difficult to accommodate within the standard *two-body* confinement force model of Lipkin-type with a universal confinement strength for baryons and compact six-quark states. In order to *model* the complex color dynamics in a compound six-quark system, we have proposed that the effective two-body confining strength in the  $d'$  is weaker than in a single nucleon (model III). We then obtain a  $d'$  mass,  $M_{d'}=2092$  MeV, which is compatible with the experimentally suggested resonance mass. In the absence of a solvable theory of confinement, our harmonic-oscillator model III should be viewed as *an attempt to model the more complicated color dynamics in a genuine six-quark system*. Our conjecture of a weaker confinement strength is based on the observation that the average distance between any pair of quarks in the  $d'$  is significantly larger than in the nucleon. In this long-range regime the confinement interaction is poorly understood. A harmonic-oscillator confinement model clearly shows the inverse relation between the size of the system and the confinement strength. If the  $d'$  is experimentally confirmed, it would be an indication that the *effective two-body* confinement strength is weaker in a genuine six-quark system with the size of the  $d'$ .

It remains to be seen whether our hypothesis of a weaker confinement strength in a compound six-quark system affects other results in the  $B=2$  sector such as  $NN$  scattering phase shifts or the deuteron electromagnetic form factors [49]. According to our experience, these observables are rather insensitive to the details of confinement, and we do not expect any qualitative changes of previous results. Nevertheless, new calculations, e.g., of deuteron observables should be carried

out to explicitly check the consequences of our conjecture.

An important test of the  $d'$  hypothesis is the simultaneous description of the mass and the free pionic decay width  $\Gamma_{d'} \approx 0.5$  MeV of the  $d'$  with the same set of parameters. Model III gives a *free*  $d'$  decay width of  $\Gamma_{d'} \approx 0.3$  MeV, which is in agreement with the experimental result [28]. In the future, a detailed analysis of the  $Nd'$  and  $d'd'$  interactions similar to the calculation of the  $NH$  [56] and  $HH$  [57] interactions, as well as a calculation of the cross section for  $d'N \rightarrow NNN$  should be done. This will provide a stringent test of whether the theoretical  $d'$  radius  $r_{d'} = 1.53$  fm is consistent with the empirical ‘‘in medium’’  $d'$  decay width  $\Gamma_{\text{medium}} \approx 5$  MeV.

On the experimental side, the search for a clear  $d'$  signature in elementary reactions, such as  $pp \rightarrow pp\pi^+\pi^-$  [12] and  $\gamma d \rightarrow pn\pi^0$  [58], has begun. The experimental search for dibaryons provides a unique chance for probing the largely unexplored and little understood phenomenon of color confinement at larger interquark distances. In this regime our traditional confinement models are likely to break down. If the existence of narrow dibaryons is confirmed, it will also have important implications for deep-inelastic electron-scattering off nuclei [59], for the equation of state of nuclear matter at higher densities, and the inner structure of neutron stars [60].

#### ACKNOWLEDGMENTS

The authors thank K. Tsushima for calculational help at the early stage of the project. Stimulating discussions on the confinement issue with H. Clement, M. Engelhardt, L. Ya. Glozman, E. Lomon, D. B. Lichtenberg, M. I. Krivoruchenko, I. T. Obukhovskiy, and M. Rosina are acknowledged. This work is supported in part by the DFG Graduiertenkolleg Mu705/3, BMBF 06 Tü 746(2) and DFG Wa1147/1-1.

#### APPENDIX

In this appendix, we present all norm and Hamiltonian kernel matrix elements necessary to diagonalize the algebraic generalized eigenvalue problem of Eq. (17). We calculate the Hamiltonian and norm kernels

$$\begin{aligned} \mathcal{H}_{ij}(s_i, s_j) &= \langle \text{GCM}_i | \mathcal{A}H | \text{GCM}_j \rangle; \\ \mathcal{N}_{ij}(s_i, s_j) &= \langle \text{GCM}_i | \mathcal{A} | \text{GCM}_j \rangle, \end{aligned} \quad (\text{A1})$$

where the abbreviation  $|\text{GCM}_i\rangle$  introduced in Eq. (16) denotes

$$\begin{aligned} |\text{GCM}_i\rangle &\equiv \frac{1}{\sqrt{4\pi}} [(1/\pi b_6^2)^{3/4}]^6 \int d\hat{s}_i \cdot [Z^{S=1, T=0, C=0} \\ &\quad \times Y^{L=1}(\hat{s}_i)]^{J=0, T=0, C=0} \\ &\quad \times \left\{ \prod_{\alpha=1}^4 \exp\left(-\frac{1}{2b_6^2} \left(\mathbf{r}_\alpha - \frac{2}{3} \frac{\mathbf{s}_i}{2}\right)^2\right) \right\} \\ &\quad \times \left\{ \prod_{\beta=5}^6 \exp\left(-\frac{1}{2b_6^2} \left(\mathbf{r}_\beta + \frac{4}{3} \frac{\mathbf{s}_i}{2}\right)^2\right) \right\}, \end{aligned}$$

$$\begin{aligned} Z^{S=1, T=0, C=0} &= [\Phi_T^{S_T=1, T_T=0} \times [211]_3^{C_T=1} \otimes \Phi_D^{S_D=0, T_D=0} \\ &\quad \times [11]_3^{C_D=1}]^{S=1, T=0} [222]_1^{C=0} \end{aligned} \quad (\text{A2})$$

In Eq. (A2)  $Z^{S=1, T=0, C=0}$  is the spin(S)-isospin(T)-color(C) wave function of the  $d'$ , where the diquark ( $S_D=0$ ,  $T_D=0$ ,  $C_D=\bar{1}$ ) and the tetraquark ( $S_T=1$ ,  $T_T=0$ ,  $C_T=1$ ) STC-wave functions are coupled to the total STC wave function of the  $d'$ , with  $S=1$ ,  $T=0$ , and total color  $C=0$  of the color singlet state  $[222]_1$ . The projection onto good angular momentum  $L=1$  of the orbital part of the matrix elements of Eq. (A1) is done after the integration over all quark coordinates shown in Fig. 4:  $\Pi_{i=1}^6 \int d\mathbf{r}_i$ . Introducing the notation  $A = 1/(2b_6^2)$ , we obtain for the orbital integrals before projection, first for the norm matrix kernels  $\mathcal{N}_{ij}$ :

$$\begin{aligned} \mathcal{N}_{ij}^D &= \exp\left(-\frac{2A}{3} (\mathbf{s}_i - \mathbf{s}_j)^2\right), \\ \mathcal{N}_{ij}^X &= \exp\left(-\frac{2A}{3} (\mathbf{s}_i^2 - \mathbf{s}_j^2)\right) \exp\left(+\frac{A}{3} \mathbf{s}_i \cdot \mathbf{s}_j\right), \\ \mathcal{N}_{ij}^{XX} &= \exp\left(-\frac{2A}{3} (\mathbf{s}_i^2 - \mathbf{s}_j^2)\right) \exp\left(-\frac{2A}{3} \mathbf{s}_i \cdot \mathbf{s}_j\right). \end{aligned} \quad (\text{A3})$$

Here and in the following,  $D$  refers to the direct kernel,  $X$  represents the one-quark-exchange diagrams for quark 4 and 6, and  $XX$  refers to the two-quark-exchange diagrams of the pairs (34)  $\leftrightarrow$  (56) in orbital space. The subscripts in the kinetic energy and the two-body interaction kernels denote the quark coordinate.

The nonprojected kernels of the kinetic energy operator  $T_i = p_i^2/2m_q = -(1/2m_q)\nabla_i^2$  read

$$\begin{aligned} T_1^D(\mathbf{s}_i, \mathbf{s}_j) &= -\frac{1}{2m_q} \left[ -3A + \frac{A^2}{9} (\mathbf{s}_i - \mathbf{s}_j)^2 \right] \mathcal{N}_{ij}^D, \\ T_6^D(\mathbf{s}_i, \mathbf{s}_j) &= -\frac{1}{2m_q} \left[ -3A + \frac{4A^2}{9} (\mathbf{s}_i - \mathbf{s}_j)^2 \right] \mathcal{N}_{ij}^D, \\ T_1^X(\mathbf{s}_i, \mathbf{s}_j) &= -\frac{1}{2m_q} \left[ -3A + \frac{A^2}{9} (\mathbf{s}_i - \mathbf{s}_j)^2 \right] \mathcal{N}_{ij}^X, \\ T_5^X(\mathbf{s}_i, \mathbf{s}_j) &= -\frac{1}{2m_q} \left[ -3A + \frac{4A^2}{9} (\mathbf{s}_i - \mathbf{s}_j)^2 \right] \mathcal{N}_{ij}^X, \\ T_4^X(\mathbf{s}_i, \mathbf{s}_j) &= -\frac{1}{2m_q} \left[ -3A + \frac{A^2}{9} (\mathbf{s}_i + 2\mathbf{s}_j)^2 \right] \mathcal{N}_{ij}^X, \\ T_6^X(\mathbf{s}_i, \mathbf{s}_j) &= -\frac{1}{2m_q} \left[ -3A + \frac{A^2}{9} (2\mathbf{s}_i + \mathbf{s}_j)^2 \right] \mathcal{N}_{ij}^X, \\ T_1^{XX}(\mathbf{s}_i, \mathbf{s}_j) &= -\frac{1}{2m_q} \left[ -3A + \frac{A^2}{9} (\mathbf{s}_i - \mathbf{s}_j)^2 \right] \mathcal{N}_{ij}^{XX}, \\ T_4^{XX}(\mathbf{s}_i, \mathbf{s}_j) &= -\frac{1}{2m_q} \left[ -3A + \frac{A^2}{9} (\mathbf{s}_i + 2\mathbf{s}_j)^2 \right] \mathcal{N}_{ij}^{XX}, \end{aligned} \quad (\text{A4})$$

$$T_6^{XX}(\mathbf{s}_i, \mathbf{s}_j) = -\frac{1}{2m_q} \left[ -3A + \frac{A^2}{9} (2\mathbf{s}_i + \mathbf{s}_j)^2 \right] \mathcal{N}_{ij}^{XX},$$

where the norm kernels  $\mathcal{N}_{ij}^X$  of Eq. (A3) have been factored out. For the two-body potential kernels depicted in Fig. 5 (for the case of the one-gluon-exchange potential), we arrive after some straightforward algebra at

$$\begin{aligned} V_{12}^D(\mathbf{s}_i, \mathbf{s}_j) &= V_{56}^D(\mathbf{s}_i, \mathbf{s}_j) = \mathcal{N}_{ij}^D \left( \frac{A}{\pi} \right)^{3/2} (4\pi) \int_0^\infty dr r^2 \\ &\quad \times \exp(-Ar^2) V(r), \\ V_{46}^D(\mathbf{s}_i, \mathbf{s}_j) &= \mathcal{N}_{ij}^D \left( \frac{A}{\pi} \right)^{3/2} (4\pi)^2 \exp\left(-\frac{A}{4}(\mathbf{s}_i + \mathbf{s}_j)^2\right) \\ &\quad \times \sum_{l,m} Y_m^l *(\hat{\mathbf{s}}_i) Y_m^l(\hat{\mathbf{s}}_j) \int_0^\infty dr r^2 \\ &\quad \times \exp(-Ar^2) V(r) i_l(Ars_i) i_l(Ars_j), \\ V_{12}^X(\mathbf{s}_i, \mathbf{s}_j) &= \mathcal{N}_{ij}^X \left( \frac{A}{\pi} \right)^{3/2} (4\pi) \int_0^\infty dr r^2 \exp(-Ar^2) V(r), \\ V_{34}^X(\mathbf{s}_i, \mathbf{s}_j) &= V_{56}^X(\mathbf{s}_i, \mathbf{s}_j) = \mathcal{N}_{ij}^X \left( \frac{A}{\pi} \right)^{3/2} (4\pi) \exp\left(-\frac{A}{4}\mathbf{s}_j^2\right) \\ &\quad \times \int_0^\infty dr r^2 \exp(-Ar^2) V(r) i_0(Ars_j), \\ V_{36}^X(\mathbf{s}_i, \mathbf{s}_j) &= V_{45}^X(\mathbf{s}_i, \mathbf{s}_j) = \mathcal{N}_{ij}^X \left( \frac{A}{\pi} \right)^{3/2} (4\pi) \exp\left(-\frac{A}{4}\mathbf{s}_i^2\right) \\ &\quad \times \int_0^\infty dr r^2 \exp(-Ar^2) V(r) i_0(Ars_i), \\ V_{46}^X(\mathbf{s}_i, \mathbf{s}_j) &= \mathcal{N}_{ij}^X \left( \frac{A}{\pi} \right)^{3/2} (4\pi)^2 \exp\left(-\frac{A}{4}(\mathbf{s}_i - \mathbf{s}_j)^2\right) \\ &\quad \times \sum_{l,m} (-)^l \cdot Y_m^l *(\hat{\mathbf{s}}_i) Y_m^l(\hat{\mathbf{s}}_j) \int_0^\infty dr r^2 \\ &\quad \times \exp(-Ar^2) V(r) i_l(Ars_i) i_l(Ars_j), \\ V_{35}^X(\mathbf{s}_i, \mathbf{s}_j) &= (\mathcal{N}_{ij}^X / \mathcal{N}_{ij}^D) \cdot V_{46}^D(\mathbf{s}_i, \mathbf{s}_j), \\ V_{12}^{XX}(\mathbf{s}_i, \mathbf{s}_j) &= V_{34}^{XX}(\mathbf{s}_i, \mathbf{s}_j) = V_{56}^{XX}(\mathbf{s}_i, \mathbf{s}_j) \\ &= \mathcal{N}_{ij}^{XX} \left( \frac{A}{\pi} \right)^{3/2} (4\pi) \int_0^\infty dr r^2 \\ &\quad \times \exp(-Ar^2) V(r), \\ V_{23}^{XX}(\mathbf{s}_i, \mathbf{s}_j) &= \mathcal{N}_{ij}^{XX} \left( \frac{A}{\pi} \right)^{3/2} (4\pi) \exp\left(-\frac{A}{4}\mathbf{s}_j^2\right) \int_0^\infty dr r^2 \\ &\quad \times \exp(-Ar^2) V(r) i_0(Ars_j), \end{aligned} \tag{A5}$$

$$\begin{aligned} V_{25}^{XX}(\mathbf{s}_i, \mathbf{s}_j) &= \mathcal{N}_{ij}^{XX} \left( \frac{A}{\pi} \right)^{3/2} (4\pi) \exp\left(-\frac{A}{4}\mathbf{s}_i^2\right) \int_0^\infty dr r^2 \\ &\quad \times \exp(-Ar^2) V(r) i_0(Ars_i), \\ V_{46}^{XX}(\mathbf{s}_i, \mathbf{s}_j) &= V_{45}^{XX}(\mathbf{s}_i, \mathbf{s}_j) = (\mathcal{N}_{ij}^{XX} / \mathcal{N}_{ij}^X) \cdot V_{46}^X(\mathbf{s}_i, \mathbf{s}_j). \end{aligned}$$

In order to project all kernels onto good angular momentum  $L=1$  in the relative coordinate, we first expand the scalar products of the generator coordinates  $(\mathbf{s}_i \cdot \mathbf{s}_j)$  appearing in the exponential functions in terms of spherical harmonics

$$\exp(-\alpha A \mathbf{s}_i \cdot \mathbf{s}_j) = 4\pi \sum_l (-)^l \hat{l} i_l(\alpha A s_i s_j) Y^l(\hat{\mathbf{s}}_i) \cdot Y^l(\hat{\mathbf{s}}_j). \tag{A7}$$

The projection may then be performed by application of the integral operator  $\hat{P}_{\text{GCM}}^{L=1} = \int d\hat{\mathbf{s}}_i d\hat{\mathbf{s}}_j Y^{L=1}(\mathbf{s}_i) Y^{L=1}(\mathbf{s}_j)$ .

In the present case ( $L=1, S=1, T=0$ ) we obtain the following expressions for the projected norm kernels:

$$\begin{aligned} \mathcal{N}_{ij}^{D,\text{proj}} &= \frac{1}{\sqrt{3}} \exp\left(-\frac{2A}{3}(\mathbf{s}_i^2 + \mathbf{s}_j^2)\right) \cdot i_1\left(\frac{4A}{3}s_i s_j\right) \cdot \langle \text{STC} \rangle, \\ \mathcal{N}_{ij}^{X,\text{proj}} &= \frac{1}{\sqrt{3}} \exp\left(-\frac{2A}{3}(\mathbf{s}_i^2 + \mathbf{s}_j^2)\right) \cdot i_1\left(\frac{A}{3}s_i s_j\right) \cdot \langle \text{STC} \rangle, \\ \mathcal{N}_{ij}^{XX,\text{proj}} &= -\frac{1}{\sqrt{3}} \exp\left(-\frac{2A}{3}(\mathbf{s}_i^2 + \mathbf{s}_j^2)\right) \cdot i_1\left(\frac{2A}{3}s_i s_j\right) \cdot \langle \text{STC} \rangle \end{aligned} \tag{A8}$$

where the short-hand notation  $\langle \text{STC} \rangle$  has been introduced to denote the reduced norm operator matrix elements  $\langle ||1|| \rangle, \langle ||\hat{P}_{46}^{\text{STC}}|| \rangle$ , and  $\langle ||\hat{P}_{35}^{\text{STC}} \cdot \hat{P}_{46}^{\text{STC}}|| \rangle$  in spin-isospin-color space. Explicit expressions are given below.

Some of the projected kinetic energy kernels are simply obtained by the substitution  $\mathcal{N}_{ij} \rightarrow \mathcal{N}_{ij}^{\text{proj}}$ . The components proportional to  $\sim (\mathbf{s}_i \cdot \mathbf{s}_j) \cdot \mathcal{N}_{ij}$  are obtained after application of the trick

$$\begin{aligned} (\mathbf{s}_i \cdot \mathbf{s}_j) \cdot \exp(-A \mathbf{s}_i \cdot \mathbf{s}_j) &= -\frac{1}{A} \left| \frac{\partial}{\partial x} \exp(-A x \mathbf{s}_i \cdot \mathbf{s}_j) \right|_{x=1}, \\ \left| \frac{\partial}{\partial x} i_1(xy) \right|_{x=1} &= y i_2(y) + i_1(y). \end{aligned} \tag{A9}$$

The replacement  $\mathcal{N}_{ij} \rightarrow \mathcal{N}_{ij}^{\text{proj}}$  applies also for most of the projected two-body potential matrix elements, except for

$$\begin{aligned} V_{46}^{D,\text{proj}}(s_i, s_j) &= \frac{(4\pi)}{\sqrt{3}} \left( \frac{A}{\pi} \right)^{3/2} \exp\left(-\frac{11A}{12}(\mathbf{s}_i^2 + \mathbf{s}_j^2)\right) \cdot \langle \text{STC} \rangle \\ &\quad \times \sum_l \left( \frac{\partial}{\partial x} i_l(x) \right) \cdot \hat{l}^2 \int_0^\infty dr r^2 \\ &\quad \times \exp(-Ar^2) V(r) i_l(Ars_i) i_l(Ars_j); \\ x &= \frac{5}{6} A s_i s_j, \end{aligned}$$

$$\begin{aligned}
V_{46}^{X,\text{proj}}(s_i, s_j) &= \frac{(4\pi)}{\sqrt{3}} \left( \frac{A}{\pi} \right)^{3/2} \exp\left( -\frac{11A}{12} (\mathbf{s}_i^2 + \mathbf{s}_j^2) \right) \cdot \langle \text{STC} \rangle \\
&\times \sum_l \left( \frac{\partial}{\partial x} i_l(x) \right) (-)^l \cdot \hat{l}^2 \int_0^\infty dr r^2 \\
&\times \exp(-Ar^2) V(r) i_l(Ars_i) i_l(Ars_j) \\
&x = \frac{5}{6} A s_i s_j,
\end{aligned} \tag{A10}$$

$$\begin{aligned}
V_{35}^{X,\text{proj}}(s_i, s_j) &= -\frac{(4\pi)}{\sqrt{3}} \left( \frac{A}{\pi} \right)^{3/2} \exp\left( -\frac{11A}{12} (\mathbf{s}_i^2 + \mathbf{s}_j^2) \right) \\
&\cdot \langle \text{STC} \rangle \sum_l \left( \frac{\partial}{\partial x} i_l(x) \right) (-)^l \cdot \hat{l}^2 \\
&\times \int_0^\infty dr r^2 \exp(-Ar^2) V(r) i_l(Ars_i) \\
&\times i_l(Ars_j); \quad x = \frac{1}{6} A s_i s_j, \\
V_{46}^{XX,\text{proj}}(s_i, s_j) &= V_{35}^{X,\text{proj}}(s_i, s_j).
\end{aligned}$$

Finally, we explicitly give the spin-isospin-color  $\langle \text{STC} \rangle$  factors for the different matrix elements, first for the norm kernel

$$\begin{aligned}
\langle (S=1, L=1) J=0, T=0 \| 1 \| (S=1, L=1) J=0, T=0 \rangle &= \sqrt{3}, \\
\langle (S=1, L=1) J=0, T=0 \| \hat{P}_{46}^{\text{STC}} \| (S=1, L=1) J=0, T=0 \rangle &= 0, \\
\langle (S=1, L=1) J=0, T=0 \| \hat{P}_{35}^{\text{STC}} \hat{P}_{46}^{\text{STC}} \| (S=1, L=1) J=0, T=0 \rangle \\
&= +\frac{\sqrt{3}}{4}.
\end{aligned} \tag{A11}$$

The same  $\langle \text{STC} \rangle$  matrix elements apply to the kinetic energy and for the one- $\sigma$ -exchange potential, because as the norm operator, these operators do not depend on isospin, spin, or

TABLE V. Spin(S)-isospin(T)-color(C) matrix elements of the interaction kernels.

Diagram	Operator $\mathcal{O}_{ij}$	$\lambda_i^a \cdot \lambda_j^a$	$\lambda_i^a \cdot \lambda_j^a \boldsymbol{\sigma}_i \cdot \boldsymbol{\sigma}_j$	$\boldsymbol{\sigma}_i \cdot \boldsymbol{\sigma}_j \boldsymbol{\tau}_i \cdot \boldsymbol{\tau}_j$
Direct	$\mathcal{O}_{12}$	$-4/\sqrt{3}$	$8/(3\sqrt{3})$	$5/\sqrt{3}$
	$\mathcal{O}_{56}$	$-8/\sqrt{3}$	$+8\sqrt{3}$	$9\sqrt{3}$
	$\mathcal{O}_{46}$	$-2/\sqrt{3}$	0	0
1 $q$ exchange	$\mathcal{O}_{12} \hat{P}_{46}^{\text{STC}}$	$1/(2\sqrt{3})$	$-2/(3\sqrt{3})$	$-5/(4\sqrt{3})$
	$\mathcal{O}_{34} \hat{P}_{46}^{\text{STC}}$	$-1/(2\sqrt{3})$	$2/(3\sqrt{3})$	$5/(4\sqrt{3})$
	$\mathcal{O}_{56} \hat{P}_{46}^{\text{STC}}$	0	0	0
	$\mathcal{O}_{36} \hat{P}_{46}^{\text{STC}}$	$-1/(2\sqrt{3})$	$2/(3\sqrt{3})$	$5/(4\sqrt{3})$
	$\mathcal{O}_{45} \hat{P}_{46}^{\text{STC}}$	0	0	0
	$\mathcal{O}_{46} \hat{P}_{46}^{\text{STC}}$	$\sqrt{3}/2$	$3\sqrt{3}/2$	0
2 $q$ exchange	$\mathcal{O}_{35} \hat{P}_{46}^{\text{STC}}$	0	$4/(3\sqrt{3})$	$5/(4\sqrt{3})$
	$\mathcal{O}_{12} \hat{P}_{46}^{\text{STC}} \hat{P}_{35}^{\text{STC}}$	$1/\sqrt{3}$	$1/\sqrt{3}$	$-3\sqrt{3}/4$
	$\mathcal{O}_{34} \hat{P}_{46}^{\text{STC}} \hat{P}_{35}^{\text{STC}}$	$-2/\sqrt{3}$	$2\sqrt{3}$	$9\sqrt{3}/4$
	$\mathcal{O}_{56} \hat{P}_{46}^{\text{STC}} \hat{P}_{35}^{\text{STC}}$	$-2/\sqrt{3}$	$2\sqrt{3}$	$9\sqrt{3}/4$
	$\mathcal{O}_{23} \hat{P}_{46}^{\text{STC}} \hat{P}_{35}^{\text{STC}}$	$-5/(4\sqrt{3})$	0	0
	$\mathcal{O}_{25} \hat{P}_{46}^{\text{STC}} \hat{P}_{35}^{\text{STC}}$	$-5/(4\sqrt{3})$	0	0
	$\mathcal{O}_{46} \hat{P}_{46}^{\text{STC}} \hat{P}_{35}^{\text{STC}}$	$1/(4\sqrt{3})$	0	$-\sqrt{3}/4$
	$\mathcal{O}_{45} \hat{P}_{46}^{\text{STC}} \hat{P}_{35}^{\text{STC}}$	$1/(4\sqrt{3})$	0	$-\sqrt{3}/4$

color. Table V collects all necessary  $\langle \text{STC} \rangle$  matrix elements for the remaining interactions. In the calculation of these matrix elements, we have made use of the well-known identities

$$\begin{aligned}
\lambda_i^a \cdot \lambda_j^a &= -\frac{2}{3} + 2\hat{P}_{ij}^C, \quad \boldsymbol{\sigma}_i \cdot \boldsymbol{\sigma}_j = -1 + 2\hat{P}_{ij}^S, \\
\boldsymbol{\tau}_i \cdot \boldsymbol{\tau}_j &= -1 + 2\hat{P}_{ij}^T,
\end{aligned} \tag{A12}$$

and also of the fractional parentage decomposition of the tetraquark and diquark wave functions to evaluate the quark exchange operator acting in the different spaces.

- 
- [1] R. Bilger *et al.*, Z. Phys. A **343**, 491 (1992).  
[2] B. V. Martem'yanov and M. G. Schepkin, JETP Lett. **53**, 139 (1991).  
[3] R. Bilger, H. A. Clement, and M. G. Schepkin, Phys. Rev. Lett. **71**, 42 (1993).  
[4] M. Bleszynski and R. J. Glauber, Phys. Rev. C **36**, 681 (1987).  
[5] G. A. Miller, Phys. Rev. C **35**, 377 (1987).  
[6] M. J. Leitch *et al.*, Phys. Rev. C **39**, 2356 (1989).  
[7] K. Föhl *et al.*, Phys. Rev. Lett. **79**, 3849 (1997).  
[8] N. Auerbach, W. R. Gibbs, J. N. Ginnocchio, and W. B. Kaufmann, Phys. Rev. C **38**, 1277 (1988).  
[9] M. A. Kagarlis and M. B. Johnson, Phys. Rev. Lett. **73**, 38 (1994).  
[10] G. J. Wagner, Prog. Part. Nucl. Phys. **34**, 345 (1994).  
[11] F. Simkovic and Amand Faessler, Few-Body Syst., Suppl. **9**, 231 (1995); A. Bobyk, Amand Faessler, and W. A. Kaminski, J. Phys. G **23**, 375 (1997).  
[12] W. Brodowski *et al.*, Z. Phys. A **355**, 5 (1996).  
[13] V. I. Kukulin, V. N. Pomerantsev, Amand Faessler, A. J. Buchmann, and E. M. Tursunov, Phys. Rev. C **57**, (1998); L. Ya. Glozman, V. I. Kukulin, and V. N. Pomerantsev, *ibid.* **45**, R17 (1992).  
[14] A. Valcarce, H. Garcilazo, and F. Fernandez, Phys. Rev. C **52**, 539 (1995).  
[15] H. Garcilazo and L. Mathelitsch, Phys. Rev. Lett. **72**, 2971 (1994).

- [16] H. Garcilazo, Phys. Rev. C **56**, 1751 (1997).
- [17] For a good review on dibaryons, see, K. K. Seth, Lect. Notes Phys. **234**, 150 (1985).
- [18] R. L. Jaffe, Phys. Rev. Lett. **38**, 195 (1977).
- [19] B. Silvestre-Brac and J. Leandri, Phys. Rev. D **45**, 4221 (1992).
- [20] E. L. Lomon, J. Phys. Colloq. **51**, C6-363 (1990).
- [21] M. Anselmino, E. Predazzi, S. Ekelin, S. Frederiksson, and D. B. Lichtenberg, Rev. Mod. Phys. **65**, 1199 (1993); D. B. Lichtenberg, E. Predazzi, D. H. Weingarten, and J. G. Wills, Phys. Rev. D **18**, 2569 (1978).
- [22] S. Fredriksson and M. Jandel, Phys. Rev. Lett. **48**, 14 (1982).
- [23] P. J. G. Mulders, A. Th. M. Aerts, and J. J. de Swart, Phys. Rev. D **21**, 2653 (1980); Phys. Rev. Lett. **40**, 1543 (1978).
- [24] L. A. Kondratyuk, B. V. Martemyanov, and M. G. Schepkin, Sov. J. Nucl. Phys. **45**, 776 (1987).
- [25] K. Johnson and C. B. Thorn, Phys. Rev. D **13**, 1934 (1976).
- [26] L. Ya. Glozman, A. J. Buchmann, and A. Faessler, J. Phys. G **20**, L49 (1994).
- [27] Georg Wagner, L. Ya. Glozman, A. J. Buchmann, and Amand Faessler, Nucl. Phys. **A594**, 263 (1995).
- [28] K. Itonaga, A. J. Buchmann, Georg Wagner, and A. Faessler, Nucl. Phys. **A609**, 422 (1996); I. T. Obukhovskiy, K. Itonaga, Georg Wagner, A. J. Buchmann, and Amand Faessler, Phys. Rev. C **56**, 3295 (1997).
- [29] A. De Rujula, H. Georgi, and S. L. Glashow, Phys. Rev. D **12**, 147 (1975).
- [30] A. Manohar and H. Georgi, Nucl. Phys. B **234**, 189 (1984).
- [31] I. T. Obukhovskiy and A. M. Kusainov, Phys. Lett. B **238**, 142 (1990); A. M. Kusainov, V. G. Neudatchin, and I. T. Obukhovskiy, Phys. Rev. C **44**, 2343 (1991).
- [32] F. Fernandez, A. Valcarce, U. Straub, and A. Faessler, J. Phys. G **19**, 2013 (1993).
- [33] A. Valcarce, A. J. Buchmann, F. Fernandez, and A. Faessler, Phys. Rev. C **50**, 2246 (1994); **51**, 1480 (1995).
- [34] J. R. Bergervoet *et al.*, Phys. Rev. C **41**, 1435 (1990).
- [35] A. J. Buchmann, E. Hernández, and Amand Faessler, Phys. Rev. C **55**, 448 (1997); Uli Meyer, A. J. Buchmann, and Amand Faessler, Phys. Lett. B **408**, 19 (1997); Georg Wagner, A. J. Buchmann, and Amand Faessler, *ibid.* **359**, 228 (1995); A. J. Buchmann, E. Hernández, and K. Yazaki, Nucl. Phys. **A569**, 661 (1994); Phys. Lett. B **269**, 35 (1991).
- [36] U. Straub, Z. Y. Zhang, K. Bräuer, A. Faessler, S.B. Khadikar, and G. Lübeck, Nucl. Phys. **A508**, 385c (1990).
- [37] H. J. Lipkin, Phys. Lett. **45B**, 267 (1973); **113B**, 490 (1982).
- [38] F. Lenz, J. T. Londergan, E. J. Moniz, R. Rosenfelder, M. Stingl, and K. Yazaki, Ann. Phys. (N.Y.) **170**, 65 (1986).
- [39] M. Fabre de la Ripelle, Phys. Lett. B **205**, 97 (1988).
- [40] E. Laermann *et al.*, Phys. Lett. B **173**, 437 (1986); H. Suganuma, S. Sasaki, and H. Toki, Nucl. Phys. **B435**, 207 (1995).
- [41] Z. Y. Zhang, Y. W. Yu, P. N. Shen, and Y. B. Dong, Nucl. Phys. **A561**, 595 (1993).
- [42] F. Wang, J. Ping, G. Wu, L. Teng, and T. Goldman, Phys. Rev. C **51**, 3411 (1995); F. Wang, G. Wu, L. Teng, and T. Goldman, Phys. Rev. Lett. **69**, 2901 (1992).
- [43] R. Bilger, H. A. Clement, and M. G. Schepkin, Phys. Rev. Lett. **72**, 2972 (1994).
- [44] Andreas Groh, M.Sc. thesis, University of Erlangen, 1996.
- [45] K. Wildermuth and Y. C. Tang, *A Unified Theory of the Nucleus* (Vieweg, Braunschweig, 1977).
- [46] Preliminary results have been reported in A. J. Buchmann, Georg Wagner, K. Tsushima, Amand Faessler, and L. Ya. Glozman, *Proceedings of the Sixth International Symposium on Meson-Nucleon Physics and the Structure of the Nucleon*, Blaubeuren/Tübingen, Germany, 1995, edited by D. Drechsel, G. Höhler, W. Kluge, and B. M. K. Nefkens [ $\pi N$ -Newsletter **10**, 60 (1995)]; A. J. Buchmann, Georg Wagner, K. Tsushima, L. Ya. Glozman, and Amand Faessler, *Proceedings of the 17th International School of Nuclear Physics on Quarks in Hadrons and Nuclei*, Erice, 1995, edited by Amand Faessler [Prog. Part. Nucl. Phys. **36**, 383 (1996)].
- [47] M. Cvetič-Krivec, B. Golli, N. Mankoč-Borštnik, and M. Rosina, Phys. Lett. **99B**, 486 (1980).
- [48] L. A. Kondratyuk, M. I. Krivoruchenko, and M. G. Schepkin, JETP Lett. **43**, 10 (1986).
- [49] K. Shimizu, Rep. Prog. Phys. **52**, 1 (1989).
- [50] It has been argued that because quark exchange between the clusters corresponds to a quark-antiquark exchange process in the crossed channel, there could be some overlap with the direct meson exchange interaction between quarks belonging to different clusters. However, it has previously been shown that for scalar ( $\sigma$ ) and pseudoscalar ( $\pi$ ) meson exchanges between quarks, the quark exchange diagrams can be added to the direct intercluster meson exchange diagrams without danger of double counting [51]. Also in a field-theoretical description of  $NN$  scattering in the quark model using Low's equations one finds that the two-quark exchange diagrams can be clearly distinguished from the colorless  $q\bar{q}$  (meson) exchange diagrams [52].
- [51] K. Yazaki, Prog. Part. Nucl. Phys. **24**, 353 (1990).
- [52] A. I. Machavariani, A. J. Buchmann, Amand Faessler, and G. A. Emelyanenko, Ann. Phys. (N.Y.) **253**, 332 (1997).
- [53] We do not attempt to justify this rather large factor of three here. This is clearly an artefact of the harmonic oscillator confinement model and should be taken with some caution in other applications. We expect that  $a_c^{(3)}/a_c^{(6)}$  will be substantially smaller for more realistic confinement models.
- [54] A. Faessler, F. Fernandez, G. Lübeck, and K. Shimizu, Nucl. Phys. **A402**, 555 (1983); A. Faessler, Prog. Part. Nucl. Phys. **13**, 253 (1985); M. Oka and K. Yazaki, in *Quarks and Nuclei*, International Review of Nuclear Physics I, edited by W. Weise (World Scientific, Singapore, 1984), p. 489.
- [55] I. T. Obukhovskiy, Few-Body and Quark-Hadronic Systems, Proceedings of the International Conference, edited by M. G. Sapojnikov and M. Kh. Khankhasaev, JINR, D4-87-692, Dubna, 1987, p. 200; I. T. Obukhovskiy and A. M. Kusainov, Sov. J. Nucl. Phys. **47**, 313 (1988); L. Ya. Glozman, N. A. Burkova, and E. I. Kuchina, Z. Phys. A **332**, 339 (1989).
- [56] T. Sakai, A. Buchmann, K. Yazaki, and K. Shimizu, Nucl. Phys. **A543**, 661 (1992).
- [57] T. Sakai, J. Mori, A. J. Buchmann, K. Shimizu, and K. Yazaki, Nucl. Phys. **A625**, 192 (1997).
- [58] D. Akhmedov and L. V. Fil'kov, Nucl. Phys. **A544**, 692 (1992); R. Bilger *et al.*, *ibid.* **A596**, 586 (1996).
- [59] C. Ciofi-degli-Atti and S. Simula, Few-Body Syst. **18**, 55 (1995).
- [60] Amand Faessler, A. J. Buchmann, M. I. Krivoruchenko, and B. V. Martemyanov, Phys. Lett. B **391**, 255 (1997); A. J. Buchmann, Amand Faessler, and M. I. Krivoruchenko, Ann. Phys. (N.Y.) **254** 109 (1997); Amand Faessler, A. J. Buchmann, and M. I. Krivoruchenko, Phys. Rev. C **56**, 1576 (1997).